NASA TM-89006

NASA TECHNICAL MEMORANDUM 89006

STRESS ANALYSIS of the CRACKED LAP SHEAR SPECIMEN: An ASTM ROUND ROBIN

W. S. JOHNSON

AUGUST 1986

NASA
National Aeronautics and
Space Administration

Langley Research Center
Hampton, Virginia 23665

STRESS ANALYSIS OF THE CRACKED LAP SHEAR SPECIMEN: AN ASTM ROUND ROBIN

by

W. S. Johnson

with appendices by

G. P. Anderson, L. P. Abrahamson, and K. L. DeVries
T. R. Brussat
B. Dattaguru and P. D. Mangalgiri
F. Erdogen and P. Joseph
R. A. Everett, Jr. and J. D. Whitcomb
W. L. Hufferd
G. E. Law
C. J. Lof
S. Mall

SUMMARY

This ASTM Round Robin was conducted to evaluate the state of the art in stress analysis of adhesively bonded joint specimens. Specifically, the participants were asked to calculate the strain-energy-release rate for two different geometry cracked lap shear (CLS) specimens at four different debond lengths. The various analytical techniques consisted of 2- and 3-dimensional finite element analysis, beam theory, plate theory, and a combination of beam theory and finite element analysis. The results were examined in terms of the total strain-energy-release rate and the mode I to mode II ratio as a function of debond length for each specimen geometry. These results basically clustered into two groups: geometric linear or geometric nonlinear analysis. The geometric nonlinear analysis is required to properly analyze the CLS specimens. The 3-D finite element analysis gave indications of edge closure plus some mode III loading. Each participant described their analytical technique and results. Nine laboratories participated.

INTRODUCTION

Many applications of adhesives result in bonded joint geometries that have complex stress states at the bondline termination. Debond initiation and growth may occur which could lead to joint failure. Because debonding is a self-similar cracking problem, it is natural to describe the phenomenon in terms of fracture mechanics. Furthermore, depending on the joint geometry and loading conditions, these stress states can result in three modes of debond growth:

(1) Opening mode I, due to tensile stress normal to the plane of the debond, results in a G_I strain- energy-release rate.

(2) Shearing mode II, due to in-plane shear stress, results in a G_{II} strain-energy-release rate.

(3) Tearing mode III, due to anti-plane shear stress, results in a G_{III} strain-energy-release rate.

The calculation of the strain energy release rate under such conditions is not trivial, especially when geometric non-linearities may exist. If standard test methods are to be developed to assess mixed mode static fracture toughness and debond propagation rates for designing adhesively bonded joints, confidence must be obtained in the methods used to calculate the mixed mode values of strain energy release rate. By comparing various analytical

approaches to common problems can one determine which techniques give acceptable answers.

This problem of calculating the strain energy release rate for adhesive joints has been address by ASTM Task Group E24.04.09 on Crack Growth in Adhesively Bonded Joints. ASTM Committee E-24 on Fracture Testing sponsors this task group. The task group was formed in 1981 to evaluate and recommend test methods for characterizing debond propagation in adhesively-bonded joints. In the beginning the task group decided that prior to conducting tests or recommending testing procedures it needed to assess the present state of the art in stress analyses that can be used to study debond propagation under mixed-mode conditions in adhesively-bonded joints. For this purpose a round robin was conducted and is described herein.

The cracked-lap-shear (CLS) specimen [1] was chosen for evaluation. The CLS specimen has been used for studying composite delamination [2, 3, 4, 5] and adhesive joint debonding [1, 6, 7]. The debond tip in the CLS specimen is predominatly loaded in mode II with approximately thirty percent mode I. The CLS specimen is representative of the mode mix found in many applications of bonded joints and was therefore chosen as an appropriate specimen for the round robin. There is no known "exact" solution for the CLS specimen. The round robin results will be compared to each other and to experimentally observed specimen behavior to see if any consensus "correct" solutions exist.

The two CLS specimen configurations analyzed are shown in Figs. 1 and 2. As shown in the figures, the difference in the two configurations is the thickness of the lap adherends. The adherends are aluminum. Table I gives the assumed material properties. Boundary conditions are also shown in Figs. 1 and 2. A 11.12 kN tensile load was applied for both specimen geometries. Perfect bonding between the adhesive and adherend was assumed. The material properties were considered to be linear elastic with no time-dependent behavior. For this round-robin effort, the debond was located at the middle of the adhesive layer although that is not usually the case in practice [7]. The debonding normally occurs near the strap adherend.

The information sought from each participant was their calculated strain-energy-release rates, G_I and G_{II}. The tearing mode GIII was reported, if available. Debond lengths of 2.54, 6.35, 25.40, and 101.60 mm were analyzed for both specimen configurations.

Table II lists the organizations and people who participated in this round robin. Also listed in the table are their techniques used to predict the strain-energy-release rates and the symbol representing each technique used in subsequent data plots. Table II also gives the appendix number for each participant. Each appendix gives details about the analysis techniques used and the resulting predictions. The techniques fall into four general classes: Closed Form, Geometric Linear Finite Element Analysis, Geometric Nonlinear Finite Element Analysis, and mixed Closed Form / Finite Element

Analysis. All reported analysis used linear elastic material properties. In this paper linear or nonlinear analysis refers to geometric linear or geometric nonlinear analysis.

PREDICTED RESULTS

Figs. 3 and 5 show the predicted values of total strain-energy-release rate, G_T, versus debond length, for the equal and unequal thickness adherend, respectively, where $G_T = G_I + G_{II} + G_{III}$. The plotted values of G_T are as calculated; however, the results are grouped according to the analysis method. The first group (going left to right) is the Closed Form results: the second group is the Geometric Linear Finite Element results; and the third group is the Geometric Nonlinear Finite Element results. The third group includes the mixed Closed Form/Finite Element Analysis method. A symbol is assigned to each prediction technique as given in Table 2. Figs. 4 and 6 show the predicted ratio of G_I/G_{II} versus debond length for the equal and unequal adherends, respectively. The plotted values of G_I/G_{II} are grouped as discussed above.

For the equal thickness adherend specimen results shown in Fig. 3, the four geometric nonlinear analyses resulted in a rather constant G_T as a function of debond length, while the geometric linear analyses resulted in a "humping" of the data with debond length. There is reasonable scatter (less than 10 percent) within each analysis approach (geometric linear or nonlinear). The 3-D geometric linear predictions ⟨◇⟩ resulted in a G_T about 10 percent higher than the

average of the 2-D geometric linear. The geometric nonlinear analysis results of Law (●) are approximately 10 percent higher than the other nonlinear results. (Notice that Law only predicted G_T at debond lengths of 2.54 and 101.6 mm). Law assumed plane stress conditions while the other participants chose plane strain conditions for their 2-D analysis. The results of Erdogan's Reissner plate theory (△) approach are very close to the 2-D geometric linear F.E. analysis while Brussat's closed-form beam theory (+) method is close to the geometric nonlinear F.E. analysis.

The data trends for the G_I/G_{II} ratio predictions of the equal thickness adherends shown in Fig. 4 is similar to those previously discussed for G_T except for the Lof's 3-D predictions (◇). Lof's G_I/G_{II} ratios are noticeably lower than those predicted by any of the other techniques.

The G_T behavior of the unequal thickness adherend shown in Fig. 5 is similar to that of the equal thickness adherend. Again the plate theory and the geometric linear analyses showed a "humping" with increasing crack length while the virtual crack extension/beam theory method and the geometric nonlinear analyses gave constant G_T with increasing crack length. Mall's (⊕) and Hufferd's (○) analysis were about 10 percent below the other two nonlinear analysis and the beam theory for some unexplained reason.

The G_I/G_{II} ratio predictions shown in Fig. 6 for the unequal thickness adherends followed the same trends as the G_T predictions

with two notable exceptions: the beam theory G_I/G_{II} ratio was much higher than that predicted by the geometric nonlinear analyses; and the combination beam theory/finite element analyses resulted in a significantly higher G_I/G_{II} ratio at 101.6 mm than at the shorter debonds.

All of the finite element analyses used Rybicki and Kanninen [9] virtual crack closure technique to calculate values of G_I and G_{II}, except for Hufferd's and Lof's. They calculated stress intensity factor, K, then converted to strain-energy-release rates.

DISCUSSION

There is excellent agreement among the 2-D geometric nonlinear analyses of the equal thickness adherends CLS specimen. The geometric nonlinear analysis of Law (●) assumed plane stress conditions while the analysis of Everett and Whitcomb (○), Mall (⊕), and Dattaguru and Mangalgiri (◑) assumed plane strain conditions. The plane stress analysis will result in G_T being $1/(1-\nu^2)$ (i.e. 1.19) higher than the plane strain analysis. This is approximately the difference observed in Fig. 3. In appendix VII, Law shows how the geometric nonlinear analysis requires several iterations to converge. He also discusses the importance of modeling the entire bondline and not just a short portion.

For the equal and unequal adherend specimens the beam theory predictions of G_T are very close to the geometric nonlinear

predictions. As seen in Figs. 4 and 6, the values of the geometric nonlinear G_I/G_{II} ratio is about the same for the equal and unequal thickness adherends specimens (0.25 and 0.225, respectively) in spite of the rather significant change in geometry. The beam theory analysis results were 0.27 and 0.36, respectively. Dattaguru, Everett, Whitcomb, and Johnson [8] have suggested that the beam theory approach is accurate for G_I/G_{II} determination for only equal thickness adherends specimens. Brussat did not include the debond length, a, in the calculation of G_T, G_I, and G_{II}; thus, these values are independent of debond length.

In Appendix I, Anderson, Abrahamson, and DeVries calculate G_T for a debond length of 50.8 mm (in addition to the four lengths requested) in the equal thickness adherend using a geometric linear analysis. The G_T at 50.8 mm was significantly higher than for the 25.4 mm debond length. This indicates that the "hump" predicted by geometric linear analysis is even higher than shown in Fig. 3, indicating a larger discrepancy between geometric linear and nonlinear analyses. In Appendix IV, Erdogen and Joseph present G_T as a continuous function of debond length, also illustrating the "humping" behavior.

In Appendix I, Anderson, Abrahamson, and DeVries presented two sets of analytical results. The first set used a rather course mesh and a G_T of 375 J/m^2 was obtained. The mesh was then refined and a value of G_T equal 213 J/m^2 resulted. This was consistent with the other 2-D linear finite element analysis. Thus, Anderson, et al. found that too course of a mesh could give poor results.

The geometric nonlinear analyses presented for the two example problems herein predicted G_T to be practically constant with debond length. This is not always true. For specimens with shorter lengths or thicker strap adherends the predicted G_T may vary with debond length [8,10]. However, the constant values of G_T with debond lenght are believed to be the correct results for these geometry specimens. Debond growth rates have been shown to be constant over crack lenght in similar geometry specimens made with adhesives shown to have growth rates that are governed by G_T [7,11]. Furthermore, in reference 8, measured displacements in a cracked lap shear specimen agreed closely with the geometric nonlinear analysis and not with the linear analysis. All of this points to the need to use a geometric nonlinear technique for analyzing the CLS specimen [4,8].

For those configurations of the CLS specimens that do show a variation in the geometric nonlinear G_T with debond length [8] , the beam theory approach will give incorrect results. This is because the beam theory will give only one value of G_T since the theory assumes an infinite specimen length.

Mall's ($\oplus$) approach models the crack tip area with finite elements to calculate strain-energy-release rate but uses the beam theory for overall specimen behavior. For equal thickness adherends specimen, Mall's results are about 5 percent above the geometric nonlinear finite element results. For the unequal thickness adherend, Mall's results for shorter crack lengths are about the same

as for the other nonlinear predictions ; however, his results are higher for the longer crack length.

Lof's (◇) results were very interesting. He used a 3-D geometrically linear finite element method. The G_T and G_I/G_{II} ratios were not very close to the 2-D analyses for reasons unknown. However, his analysis showed that G_I and G_{II} varied across the width of the specimen and that a G_{III} existed near the edges of the specimen. The G_T remains fairly constant across the width of the specimen while the G_I, G_{II}, and G_{III} components vary. The edge closure discussed by Lof is quite surprising. The effects of edge closure, which is obtained only by the 3-D analysis, needs to be further studied.

CONCLUSIONS

Fracture mechanics is being used to describe static toughness and damage growth behavior in adhesively bonded joints. Because the stress states at the crack tip in a bonded joint can be complex and result in several potential modes of crack propagation, it is critical that the joint specimens be analyzed properly in order to insure correct interpretation of experimental test results. To aid in evaluating potential techniques for analyzing bonded joints, ASTM Committee E-24 sponsored a round robin stress analysis of the cracked-lap-shear specimen. The participants were asked to calculate the strain-energy-release-rate at four different debond lengths on two different geometry specimens. The results of this

round robin yielded the following conclusions:

1. There was good lab-to-lab consistency of predictions between analytical techniques of the same type. For example, all of the 2-D geometric linear techniques gave results within 5 percent of each other. These results suggest that although no generally applicable closed form solutions exists for the cracked lap shear specimen, good consistent results can be obtained by properly using finite element techniques.

2. The geometric nonlinear analysis techniques give results that are most consistant with observed experimental behavior and should therefore be used for analyzing the cracked lap shear specimen.

3. Brussat's beam theory approach gives a good closed-form approximation of total strain-energy-release rate for the example CLS specimens. However, beam theory does a poor job of predicting G_I/G_{II} ratio when the adherends are of different thickness.

4. Care must be taken to ensure proper modeling of the specimen in order to get correct results. For example, the adhesive bondline must be modeled with proper grid density (as discussed by Anderson, et al.) Also, the full bondline, not just the near crack-tip region, needs to be included in the model (as discussed by Law).

5. The three dimensional analysis showed that an edge closure effect may be present at the debond front of the cracked lap shear specimen. This analysis also indicated that a small amount of G_{III} was present near the edge. The G_T remains nearly constant across the debond front although the mixture of G_I, G_{II}, and G_{III} varied. This three-dimensional effect discussed by Lof needs to be studied further.

REFERENCES

[1] Brussat, T. R., Chiu, S. T., and Mostovoy, S., "Fracture Mechanics for Structural Adhesive Bonds," AFML-TR-77-163, Air Force Materials Labora tory, Wright-Patterson AFB, Ohio, 1977.

[2] Wilkins, D. J., "A Comparison of the Delamination and Environmental Resistance of a Graphite-Epoxy and a Graphite-Bismaleimde," NAV-DG-0037, Naval Air Systems Command, September 1981. (DTIC ADA-112474).

[3] Russell, A. J., and Street, K. N., "Moisture and Temperature Effects on the Mixed-Mode Delamination Fracture of Unidirectional Graphite/Epoxy," Delamination and Debonding of Materials, ASTM STP 876, W. S. Johnson, Ed., American Society of Testing and Materials, 1985.

[4] Law, G. E., and Wilkins, D. J., "Delamination Failure Criteria for Composite Structures," NAV-GD-0053, Naval Air Systems Command, Washington, DC, 15 May 1984.

[5] Johnson, W. S. and Mangalgiri, P. D., "Influence of Resin on Interlaminar Mixed-Mode Fracture," NASA TM 87571, National Aeronautics and Space Administration, Washington, DC, July 1985.

[6] Romanko J., Liechti, K. M., Knauss, W. G., "Integrated Methodology for Adhesive Bonded Joint Life Predictions," AFWAL-TR-82-4139, Air Force Wright Aeronautical Laboratories, Wright-Patterson AFB, OH, 1982.

[7] Mall, S., Johnson, W. S., and Everett, R. A., Jr., "Cyclic Debonding of Adhesively Bonded Composites," Adhesive Joints , K. L. Mittal, Ed., Plenum Press, New York, 1984, pp. 639-658.

[8] Dattaguru, B., Everett, R. A., Jr., Whitcomb, J. D., and Johnson, W. S., "Geometrically Non-Linear Analysis of Adhesively Bonded Joints," Journal of Engineering Materials and Technology , January 1984, Vol. 106, pp. 59-65.

[9] Rybicki, E. F., and Kanninen, M. F., "A Finite Element Calculation of Stress Intensity Factory by a Modified Crack Closure Integral," Engineering Fracture Mechanics, Vol, 9, No. 4, 1977, pp. 931-939.

[10] Everett, R.A. ,Jr. and Johnson, W. S., "Repeatability of Mixed Mode Adhesive Debonding", Delamination and Debonding of Materials, ASTM STP 876, W.S. Johnson, Ed., American Society for Testing and Materials, Philadelphia, pp. 267-281.

[11] Mall, S. and Johnson, W.S., "Characterization of ModeI and Mixed-Mode Failure of Adhesive Bonds Between Composite Adherends", Composite Materials:Testing and Design (Seventh Conference),ASTM STP 893, J.M. Whitney, Ed., American Society of Testing and Materials, Philadelphia, 1986,pp. 322-334.

Table I. - Material Properties

	Aluminum adherend	Adhesive
E	72450 MPa	1932 MPa
ν	0.33	0.40

TABLE II - ROUND ROBIN ANALYSES & PARTICIPANTS

ANALYSIS	NAME	ORGANIZATION	TECHNIQUE/MODEL	SYMBOL	APPENDIX
CLOSED FORM	T. R. BRUSSAT	LOCKHEED-CALIFORNIA CO.	BEAM THEORY	+	II
	F. ERDOGAN P. JOSEPH	LEHIGH UNIVERSITY	REISSNER PLATE THEORY	△	IV
GEOMETRIC LINEAR	G. P. ANDERSON/ L. P. ABRAHAMSON K. L. DEVRIES	THIOKOL CORPORATION/ UNIVERSITY OF UTAH	F. E. TASS	◨	I
	R. A. EVERETT J. D. WHITCOMB	NASA LANGLEY	F. E. GAMNAS	□	V
	W. L. HUFFERD	UNITED TECHNOLOGIES-CSD	F. E. TEXGAP	■	VI
	C. LOF	NATIONAL AEROSPACE LAB. NLR (THE NETHERLANDS)		◇	VIII
GEOMETRIC NONLINEAR	B. DATTAGURU/ P. MANGALGIRI	INDIAN INSTITUTE OF SCIENCE	F. E. GAMNAS (EAST)	◑	III
	W. L. HUFFERD	UNITED TECHNOLOGIES-CSD	F. E. VISTA	⌀	VI
	G. E. LAW	GENERAL DYNAMICS/FW	F. E. NASTRAN	●	VII
	R. A. EVERETT J. D. WHITCOMB	NASA LANGLEY	F. E. GAMNAS	○	V
MIXED	S. MALL	U. OF MISSOURI-ROLLA	BEAM THEORY + LINEAR F. E. GEOMETRIC NONLINEAR	⊕	IX

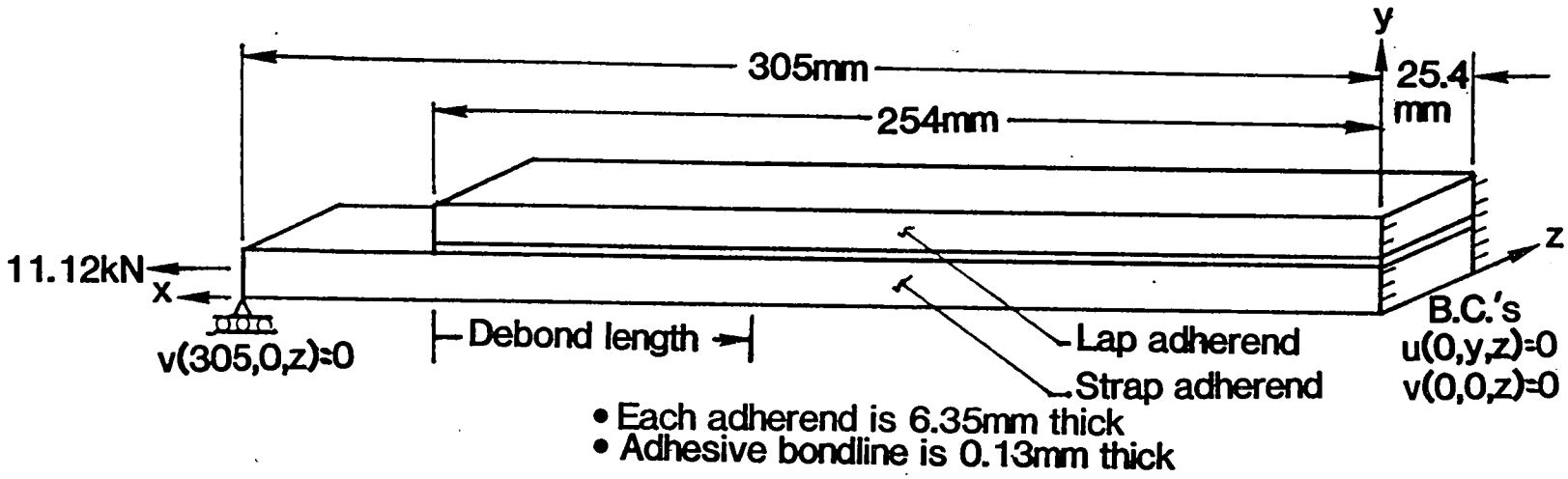

Figure 1 - Equal thickness adherend specimen

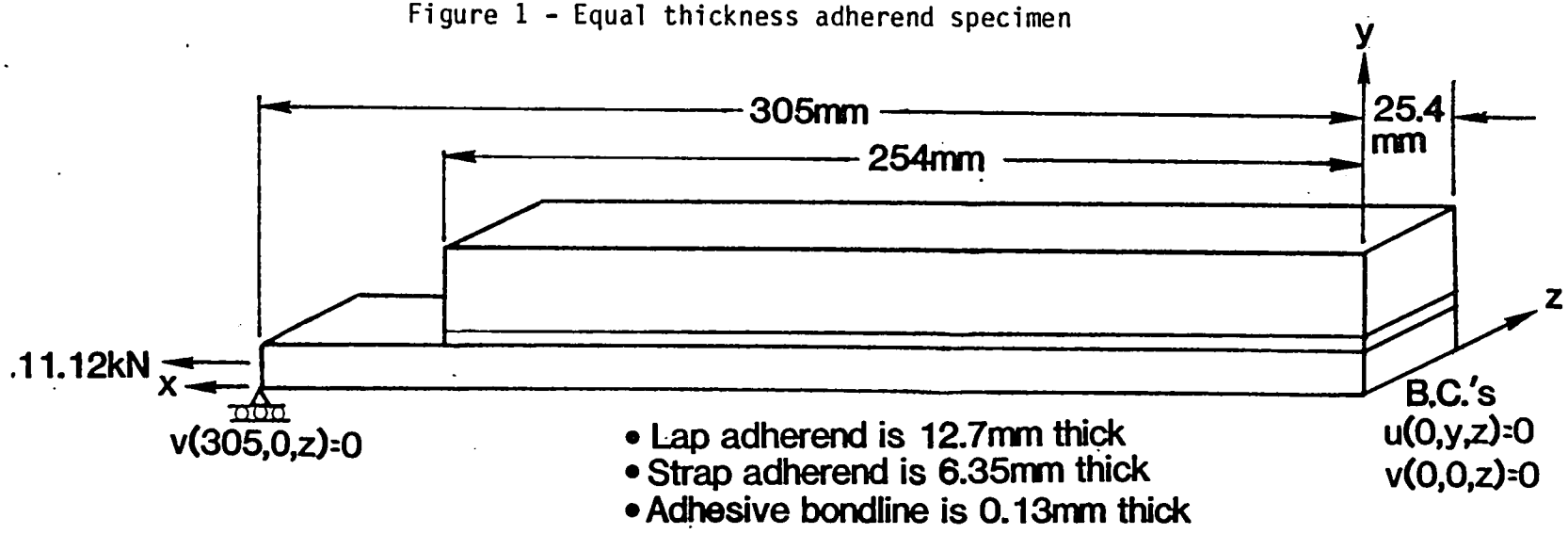

Figure 2 - Unequal thickness adherend specimen

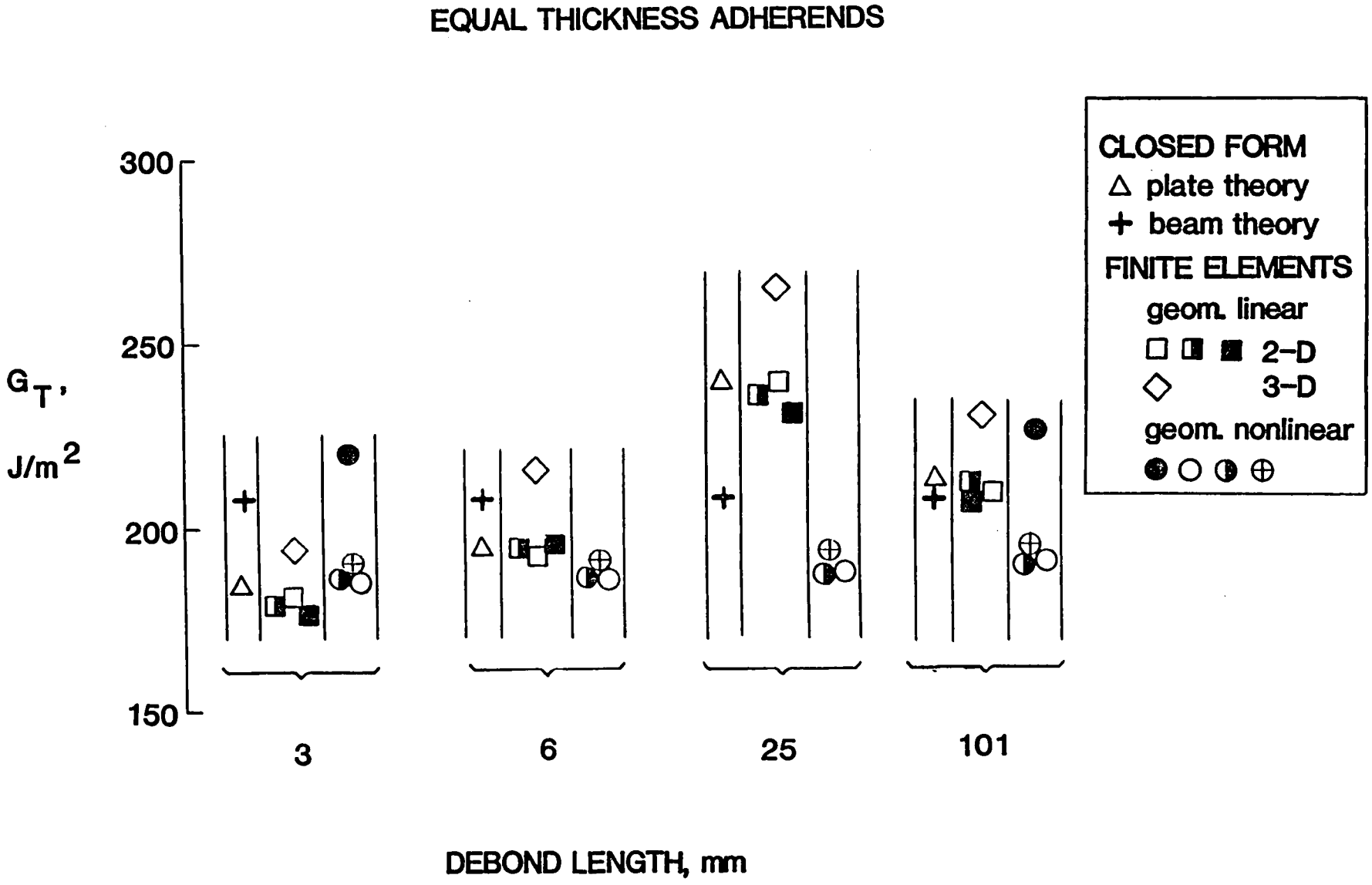

Figure 3 - Predicted total strain energy release rate versus debond length for equal thickness adherend specimens.

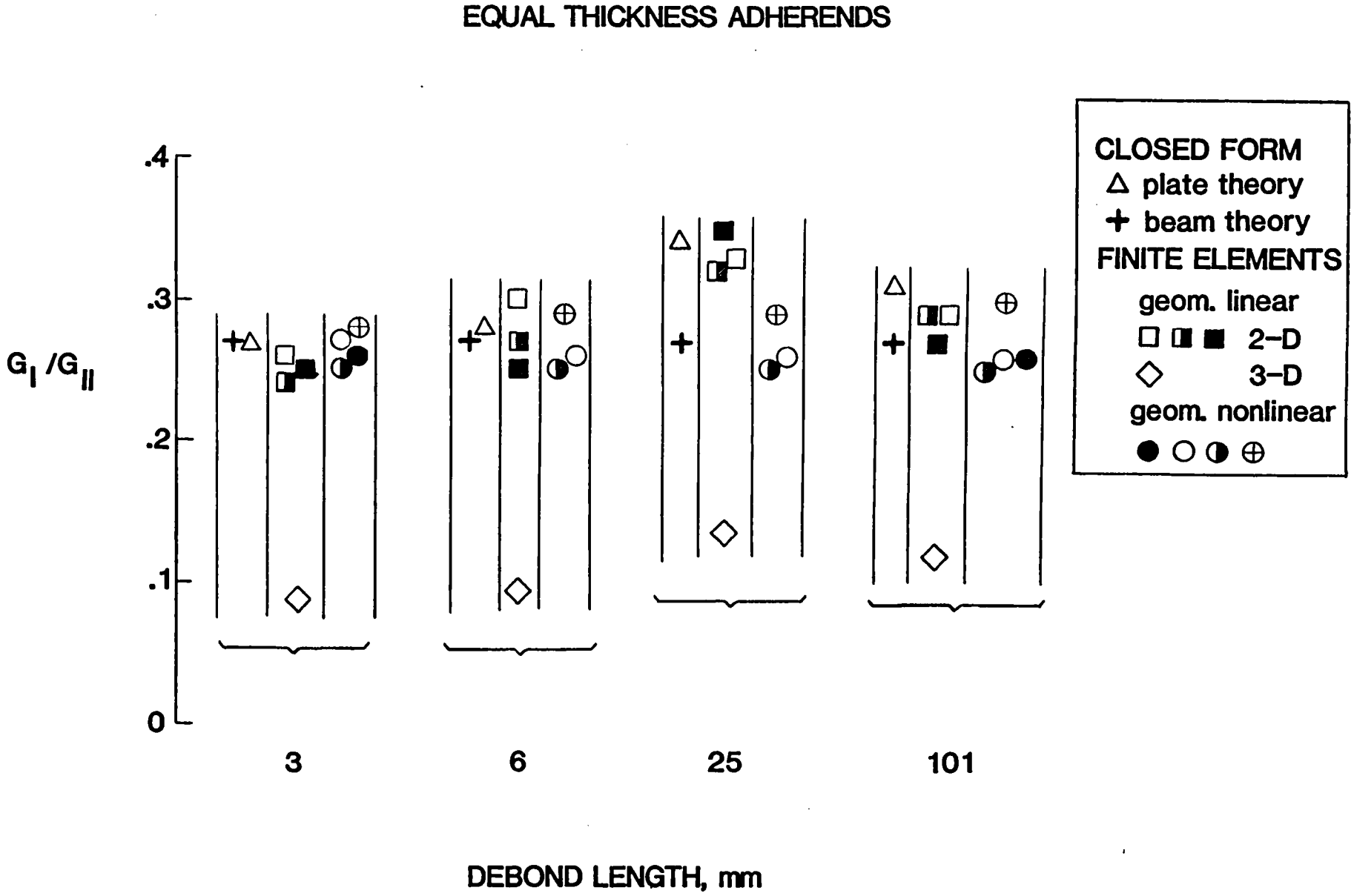

Figure 4 - Predicted ratio of mode I to mode II versus debond length for equal thickness adherend specimens.

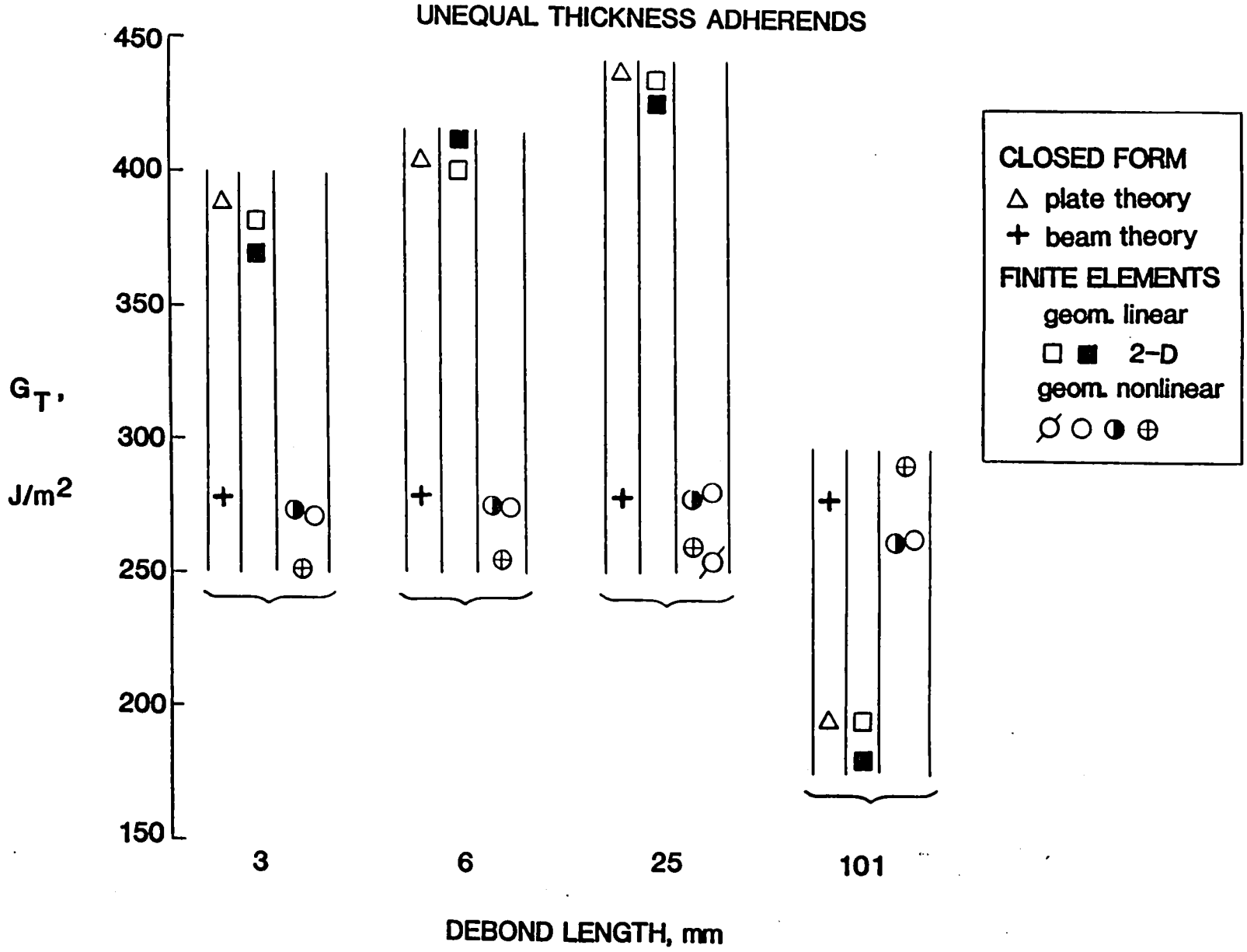

Figure 5 - Predicted total strain energy release rate versus debond length for unequal thickness adherend specimens.

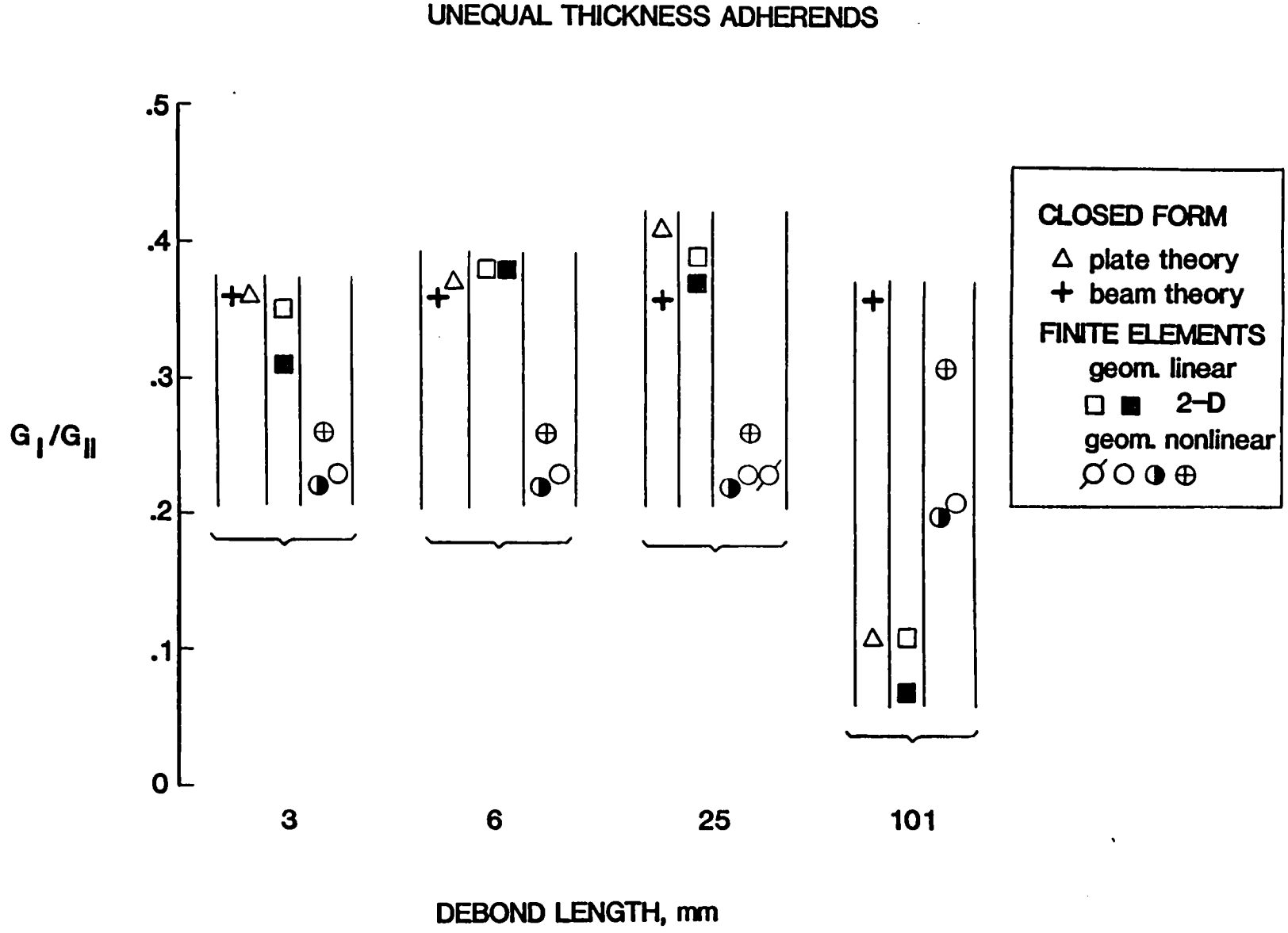

Figure 6 - Predicted ratio of mode I to mode II versus debond length for unequal thickness adherend specimens.

APPENDIX I

G. P. Anderson and L. P. Abrahamson
Thiokol Corporation
Brigham City, Utah

and

K. L. DeVries
Department of Mechanical and Industrial Engineering
University of Utah
Salt Lake City, Utah

APPROACH

The analysis of the equal thickness adherend cracked-lap-shear specimen (CLS-A) was completed using a linear elastic finite element computer program (TASS - generated by Morton Thiokol, Inc.). No special crack tip elements were used. A thin row of elements was input at the center of the adhesive; a crack was simulated by replacing these elements with "void" elements (that is, a zero or near zero stiffness element).

Mode I and mode II energy release rates (G_I and G_{II}) were calculated using the modified crack closure method outlined in the reference below. The grid network consisted of 1,710 quadrilateral elements, three elements through the thickness of each adherend and seven through the adhesive. Each quadrilateral element was automatically divided into four linear displacement elements by the computer to calculate grid displacements. The grid network as shown in Fig. I-1 contained 0.003 in. × 0.0008 in. quadrilateral elements near the crack tip.

The modified crack closure method required the two equations:

$$G_I = \frac{F_y(u_{y1} - u_{y2})}{2\Delta a}$$

$$G_{II} = \frac{F_x(u_{x1} - u_{x2})}{2\Delta a}$$

where F_x and F_y are the forces required to close the crack a distance Δa and u_{xi}, u_{yi} are the x and y crack opening displacements a distance Δa behind the crack tip [I-1].

RESULTS

The resulting energy release rates for five crack depths are presented in Table I-1.

The initial analysis for the 101.6 mm (4 in.) crack depth used a linear displacement element and the grid shown in Fig. I-2. A total energy release rate of 375 J/m^2 was obtained. It was later determined that the grid network between $x = 50.8$ and $x = 139.7$ mm was too coarse to provide an adequate beam bending analysis. The proper energy release rate (213 J/m^2) was obtained by using a quadratic displacement element with a coarse grid similar to Fig. I-2 or by using a finer grid (Fig. I-1) with the linear displacement element. The grid in Fig. I-2 used 1,710 elements while the grid in Fig. I-1 required 2,347 elements. The quadratic displacement element grid used 640 eight-node elements.

REFERENCES

[I-1] Rybicki, E. F. and Kanninen, M. F.: "A Finite Element Calculation of Stress Intensity Factors by a Modified Crack Closure Integral", Engineering Fracture Mechanics, Vol. 9, pp. 931-938, 1977.

TABLE I-1

Calculated Strain Energy Release Rates
With Debond In Middle Of Adhesive

J/m^2

Debond Length					
in.	0.10	0.25	1.0	2.0	4.0
mm.	2.54	6.35	25.40	50.80	101.60
CLSA					
G_I	35	42	57	95	48
G_{II}	144	153	180	234	165
G_T	179	195	237	329	213

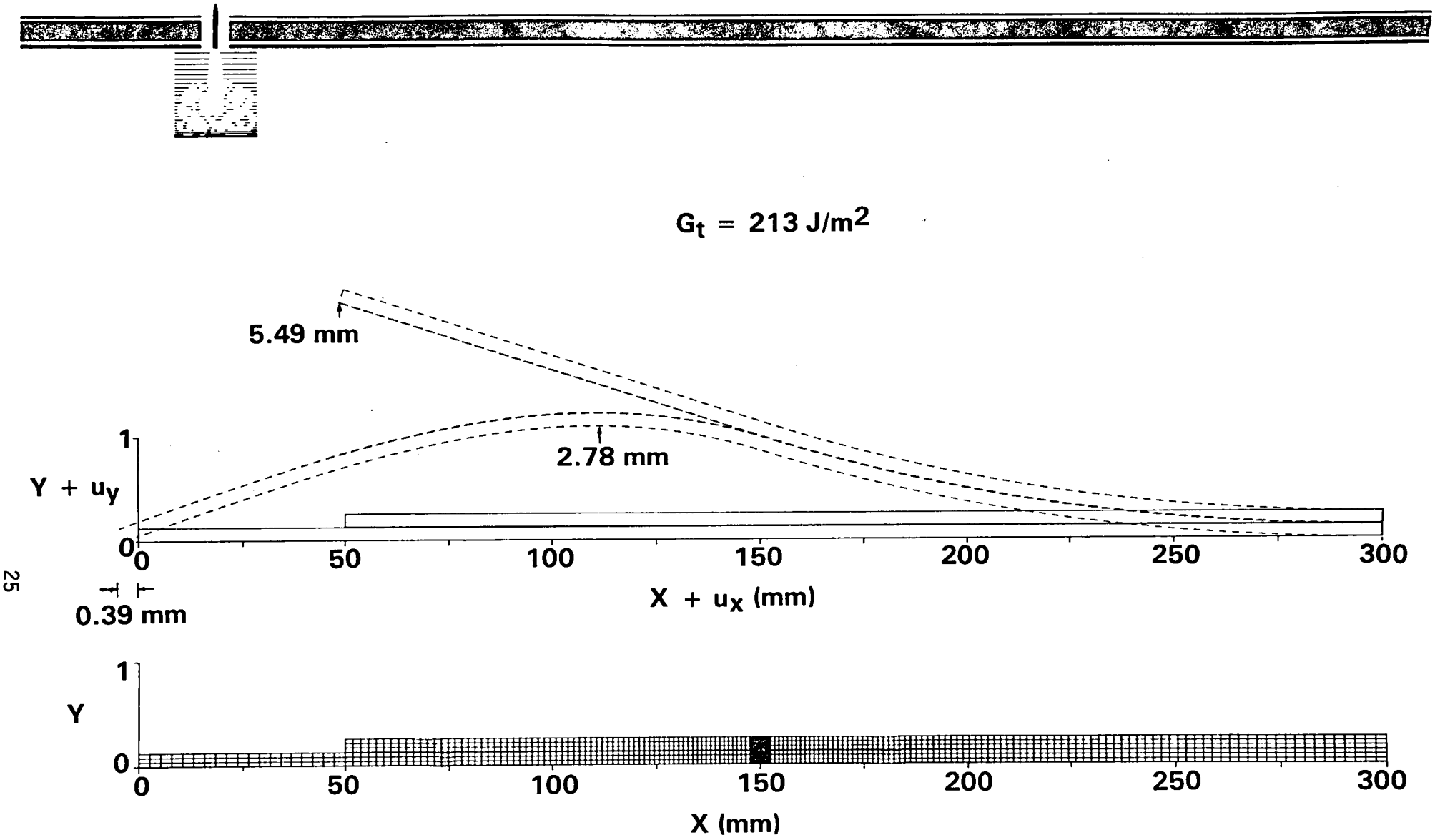

Figure I-1. Cracked lap shear specimen-refined grid.

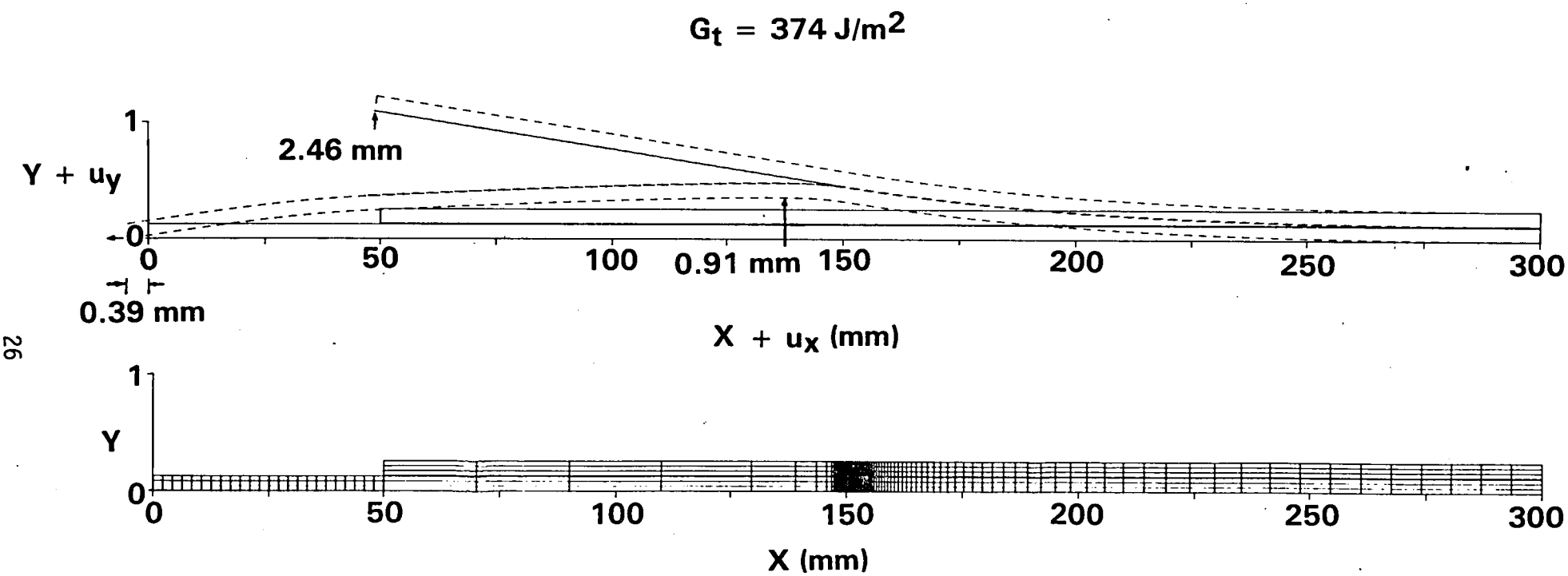

Figure I-2. Cracked lap shear specimen-initial grid.

APPENDIX II

T. R. Brussat
Lockheed-California Company
Burbank, CA 91520

APPROACH

Using elementary beam theory closed-form analytical solutions were obtained for the mode I and mode II components of the strain-energy-release rate for both CLS specimen geometries.

Reference II-1, which first introduced the CLS specimen, provides most of the equations used here. The assumption is made in Ref. II-1 that the length of the specimen and crack are large compared to the thicknesses; consequently the equations are all independent of crack length.

The adhesive layer is relatively flexible and relatively thin. The contribution of adhesive stiffness can therefore be neglected. However, the bondline thickness does significantly affect the offset distance characterizing the crack-tip eccentricity, and it also significantly affects the moment of inertia on the uncracked end of the specimen. Therefore, bondline thickness is considered in calculating these quantities.

Analytical Equations

An exact expression for total strain-energy-release rate of an infinite-length CLS specimen is derived in Ref. II-1. The resulting Equation is

$$G_T = \frac{P^2}{2b_N(EA)_2}\left[1 - \frac{(EA)_2}{(EA)_o}\right] \qquad \text{(II-1)}$$

where P is the applied load; b_N is the specimen width (measured at the bondline); $(EA)_2$ is the tensile rigidity of the strap; and $(EA)_o$ is the total tensile rigidity (lap + strap).

Ordinary beam theory is used in Ref. II-1 to obtain expressions for the mode I crack opening displacements and the limiting value of the internal bending moment at the crack tip for the infinite-length specimen. The derivation presented in Ref. II-1 could have been modified to satisfy the round-robin boundary conditions (i.e. specimen length and loading conditions), but for simplicity this was not attempted. The expressions given in Ref. II-1 are given in terms of two dimensionless parameters, γ_2 and γ_0, which are related as follows to the bending rigidities $(EI)_2$ and $(EI)_0$ of the strap section and the combined (lap + strap) section, respectively:

$$\lambda_2 = \sqrt{p/(EI)_2}$$

$$\lambda_0 = \sqrt{p/(EI)_0} \qquad \text{(II-2)}$$

The mode I crack opening displacement a distance x from the crack tip is given by

$$y' = \frac{\bar{y}_2 - \bar{y}_0}{1 + (\lambda_2/\lambda_0)} = \left(e^{-\lambda_2 x} + \lambda_2 x - 1 \right) \qquad \text{(II-3)}$$

where $\bar{y}_2$ is the centroid location of the strap section, and $\bar{y}_0$ is the centroid location of the combined section. The limiting value of internal bending moment at the crack tip is

$$M_0 = \frac{(\bar{y}_2 - \bar{y}_0)P}{1 + (\lambda_2^0/\lambda_0)} \qquad \text{(II-4)}$$

An approximation for the mode I component of strain-energy-release rate is derived in Ref. II-1 under the following assumptions:

(1) G_I for a CLS specimen in tension is equal to G_I for a CLS specimen subjected to end moments of magnitude M_o.

(2) $G_{II}/G_T = 4/7$ for the CLS specimen in pure bending. (This is the exact beam-theory result for equal thickness adherends and a zero-thickness adhesive layer).

In accordance with these two assumptions, the Equation for G_I given in Ref. II-1 is

$$G_I = \frac{2M_o^2}{7b_N(EI)_2}\left[1 - \frac{(EI)_2}{(EI)_o}\right] \qquad \text{(II-5)}$$

Recently the author has re-examined the second assumption above. For purposes of the round-robin analysis study, a second way of estimating G_I was proposed, based on the following alternative assumption:

The problem of the CLS specimen in pure bending can be separated into the approximately Pure mode I and approximately Pure mode II problems shown in Fig. II-1.

The pure bending of the CLS specimen under end moments, M_o, is shown in Fig. II-1(a). In (b) the moment M_o is balanced by a pair of moments, M_1 applied to the lap and M_2 applied to the strap. The magnitudes of M_1 and M_2 are each proportional to the ratio of the bending rigidity divided by the centroidal distance from the bondline, $(EI)_1/|y_1|$ and $(EI)_2/|y_2|$ respectively. This creates equal and opposite bending strains along the two faces

of the crack, which is an antisymmetric condition. The magnitudes of M_1 and M_2 are given by

$$M_1 = \frac{M_o(EI)_1/|y_1|}{(EI)_1/|y_1| + (EI)_2/|y_2|}$$

$$M_2 = \frac{M_o(EI)_1/|y_2|}{(EI)_1/|y_1| + (EI)_2/|y_2|} \qquad \text{(II-6)}$$

In Fig. II-1(c), an approximately pure mode I case is shown such that superposition of (b) and (c) would lead to (a). Thus, the solution G_I for the case shown in Fig. II-1(c) is an alternative approximate solution for G_I for the CLS specimen loaded in tension. Tada, et al., (Ref. II-2) give the following solution for the configuration shown in Fig. II-1(c):

$$G_I = \frac{M_1^2}{2b_N}\left[\frac{1}{(EI)_1} + \frac{1}{(EI)_2}\right] \qquad \text{(II-7)}$$

In the results that follow, Method 1 uses Eq. (II-5) to estimate G_I, while Method 2 uses Eqs. (II-6) and (II-7).

G_{III} vanishes in this 2-dimensional analysis. Therefore, the mode II strain-energy-release rate can be estimated by subtraction:

$$G_{II} = G_T - G_I \qquad \text{(II-8)}$$

The relative sliding-mode displacements, Δx, between the crack surfaces result additively from the tensile load and bending moment in the strap; the

lap is assumed to be stress-free. From the beam theory analysis results given in Ref. II-1 it can easily be shown that

$$\Delta x = \frac{Px}{(EA)_2} + \frac{h_2 M_o}{2(EI)_2 \lambda_2} \left(1 - e^{-\lambda_2 x}\right) \qquad \text{(II-9)}$$

where h_2 is the thickness of the strap.

RESULTS AND DISCUSSION

Table II-1 gives the strain-energy-release rate components for CLS A and CLS B.

Note that the two different methods of estimating G_I give very different results for the unequal adherend case, CLS B. Eq. (II-5) (Method 1) results in a G_I/G_{II} ratio of 0.36, whereas Eq. (II-7)(Method 2) gives $G_I/G_{II} = 0.54$.

Since the supporting assumptions for Method 2 seem more valid, but the results for Method 1 seem more likely to be correct, it is of interest to submit both for the round-robin study.

REFERENCES

[II-1] Brussat, T. R, Chiu, S. T., and Mostovoy, S.: "Fracture Mechanics for Structural Adhesive Bonds - Final Report," AFML-TR-77-163, Air Force Materials Laboratory, Wright-Patterson AFB, Ohio, Oct. 1977.

[II-2] Tada, H., Paris, P. C., and Irwin, G. R.: "The Stress Analysis of Cracks Handbook," Del Research Corp., Hellerton, PA 1973.

TABLE II-1

Calculated Values of Strain Energy Release Rate

J/m^2

	CLSA		CLSB	
	Method I	Method II	Method I	Method II
G_I	44	44	74	97
G_{II}	164	164	204	181
G_T	208	208	278	278
G_I/G_{II}	0.27	0.27	0.36	0.54

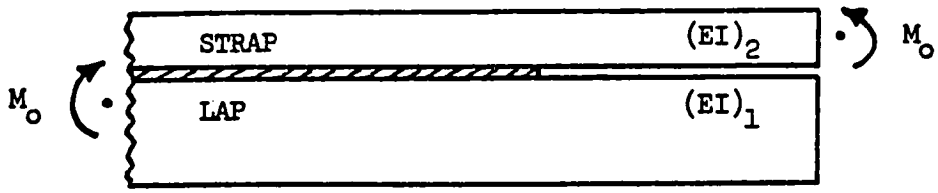

(a) CLS in Pure Bending

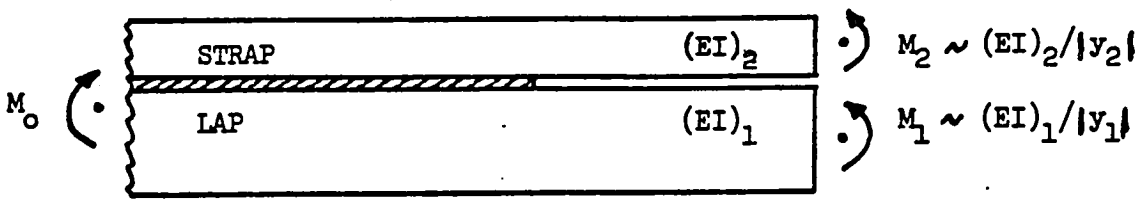

(b) Approximately Pure Mode II

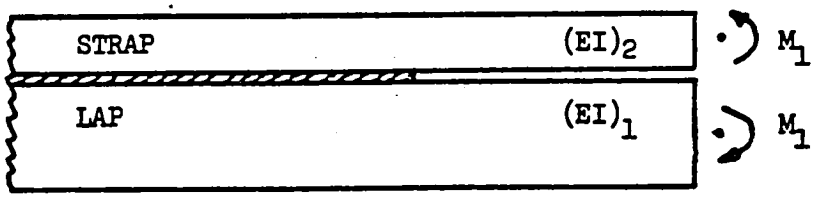

(c) Approximately Pure Mode I

Figure II-1. Approximately symmetric and antisymmetric components for the CLS specimen bending.

APPENDIX III

B. Dattaguru and P. D. Mangalgiri
Department of Aerospace Engineering
Indian Institute of Science
Banagalore, India

APPROACH

A Finite Element Analysis was carried out on a two dimensional plane strain idealization of the cross-section of these joints. The eccentricity of load transfer in these joints causes large rotations and so a geometrically nonlinear finite element analysis was employed (Refs. III-1, III-2, and III-3). The basic approach used was Lagrangian where the displacements are referred to the underformed configuration of the structure. The geometric nonlinearity was introduced in the strain-displacement relations as

$$\varepsilon_x = \frac{\partial u}{\partial x} + \frac{1}{2}\left[\left(\frac{\partial u}{\partial x}\right)^2 + \left(\frac{\partial v}{\partial x}\right)^2\right]$$

$$\varepsilon_y = \frac{\partial v}{\partial y} + \frac{1}{2}\left[\left(\frac{\partial u}{\partial y}\right)^2 + \left(\frac{\partial v}{\partial y}\right)^2\right] \qquad \text{(III-1)}$$

$$\gamma_{xy} = \frac{\partial u}{\partial y} + \frac{\partial v}{\partial x} + \frac{\partial u}{\partial x}\frac{\partial u}{\partial y} + \frac{\partial v}{\partial x}\frac{\partial v}{\partial y}$$

where u and v are displacements along x and y axes. Isoparametric elements were used. The tangent stiffness matrix at any stage of deformation was calculated as

$$K_T = K_o + K_L + K_g \qquad \text{(III-2)}$$

where K_o, K_L and K_g are the linear, large displacement and geometric stiffness matrices. A Newton-Raphson iterative scheme was employed and the tangent stiffness metrix was updated after every four iterations.

CALCULATIONS OF G_I AND G_{II}

The mode I and mode II strain-energy-release rates G_I and G_{II} were calculated based on virtual crack extension method (Ref. III-4). In order to account for large rotation of the debond, the components of forces and displacements in the directions along and normal to the center line of the deformed debond configuration were used to calculate G_I and G_{II} (Fig. III-1). Thus

$$G_I = \frac{1}{2} P_{y'} \frac{(v'_2 - v'_3)}{b \Delta a}$$

$$G_{II} = \frac{1}{2} P_{x'} \frac{(u'_2 - u'_3)}{b \Delta a} \qquad \text{(III-3)}$$

where u' and v' are displacements along x' and y' axes as shown in Fig. III-1.

Finite Element Model

A typical finite element mesh used for the present analysis is shown in Fig. III-2. The mesh has 371 nodes and 320 elements. Other models varied between 305 to 375 nodes and 258 to 320 elements. In all the models, the thin adhesive was divided into two layers of elements across the thickness. The applied loading was assumed to be uniform on the loaded end and was distributed as a consistent load vector at the nodes.

NUMERICAL RESULTS

Analysis was carried out for debond lengths a = 0.1, 0.25, 1.0 and 4.0 in. The strain-energy-release rates for all these cases are shown in Table III-1.

REFERENCES

[III-1] Zeinckiwicz, O. C.: The Finite Element Method in Engineering Science. Second Edition, McGraw-Hill, New York, 1971.

[III-2] Whitcomb, J. D.: Finite Element Analysis of Instability - Related Delamination Growth. NASA TM-81964, 1981.

[III-3] Dattaguru, B.; Everett, R. A., Jr.; Whitcomb, J. D.; and Johnson, W. S.: Geometrically Nonlinear Analysis of Adhesively Bonded Joints. Journal of Engineering Materials and Technology, Vol. 106, Jan. 1984, pp. 59-65.

[III-4] Rybicki, E. F.; and Kanninen, M. F.: A Finite Element Calculation of Stress Intensity Factors by a Modified Crack Closure Integral, Eng. Fract. Mech., Vol. 9, 1977, pp. 931-938.

TABLE III-1

Calculated Strain Energy Release Rates
With Debond In Middle Of Adhesive

J/m^2

Debond Length,				
in.	0.10	0.25	1.0	4.0
mm.	2.54	6.35	25.40	101.60
CLSA				
G_I	37	37	37	38
G_{II}	150	150	151	153
G_T	187	187	188	191
CLSB				
G_I	49	49	50	44
G_{II}	224	225	227	218
G_T	273	274	277	262

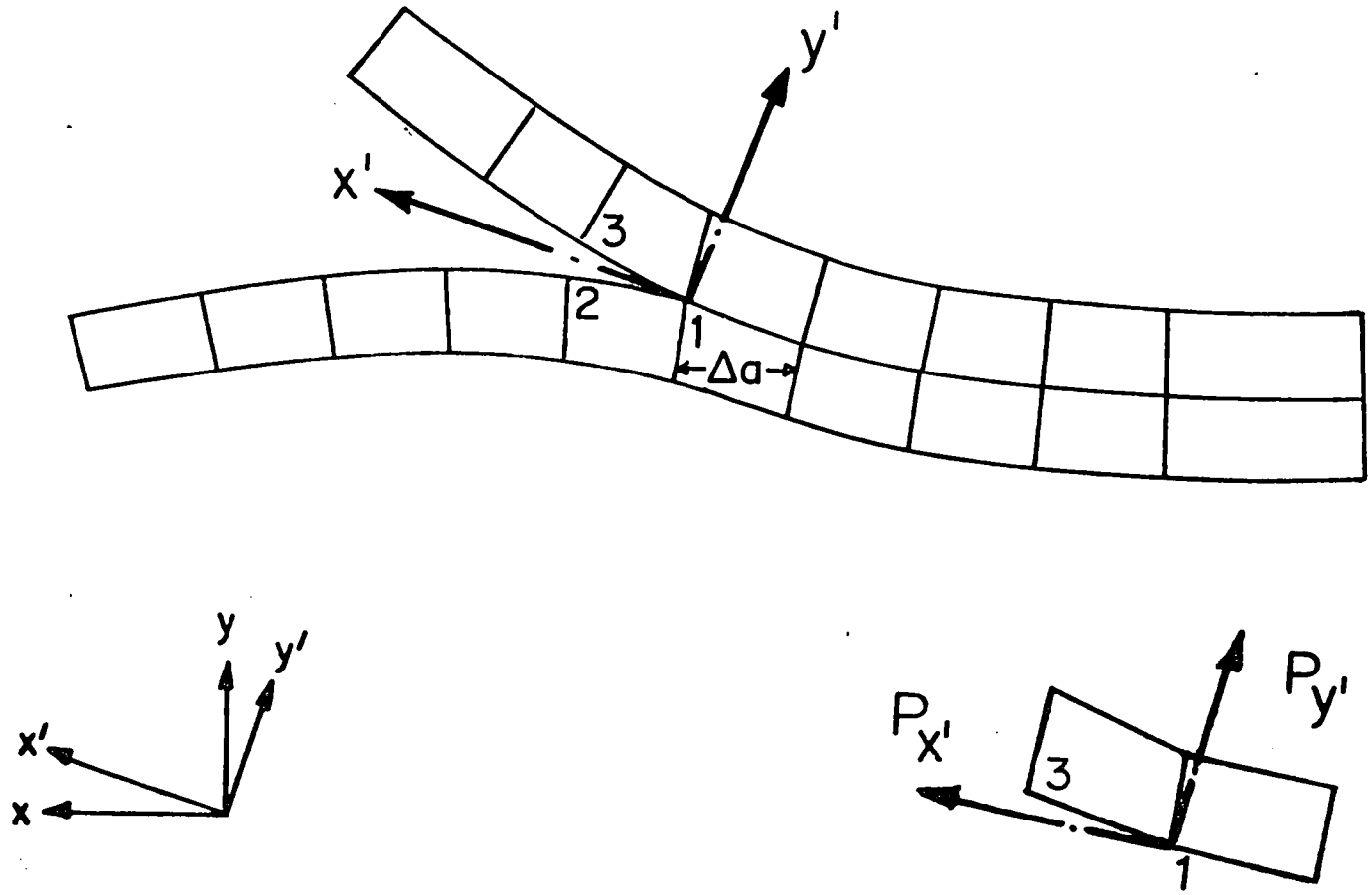

Figure III-1. Transformed coordinate system for G calculations.

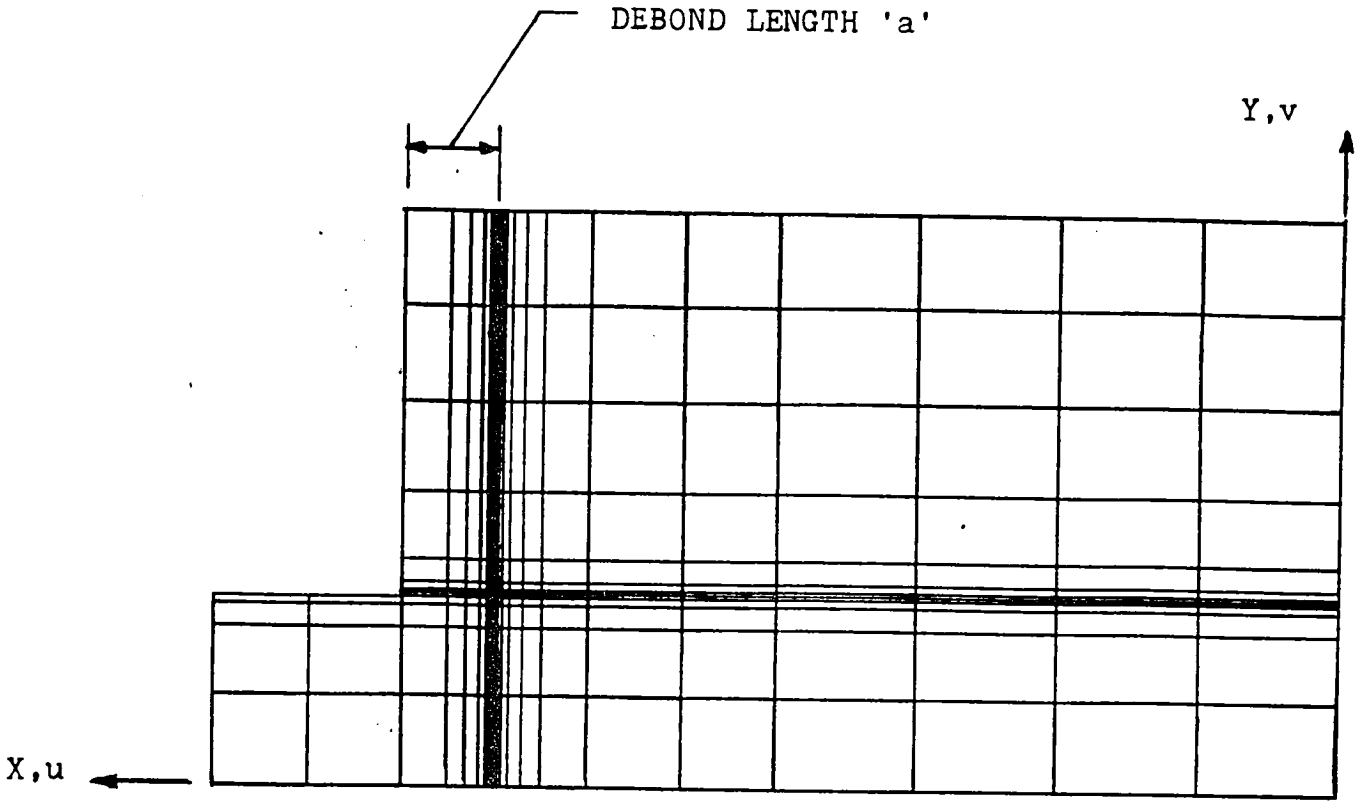

Figure III-2. A typical finite element mesh.

APPENDIX IV

F. Erdogen and P. Joseph
Lehigh University, Bethlehem, PA 18015

ASSUMPTIONS

The stress analysis of the round robin cracked-lap-shear specimens is solved under the following assumptions:

(a) The adherends are approximated by Reissner plates. That is a plate theory taking into account the transverse shear effects rather than continuum elasticity is used in formulating the problem.

(b) The problem is assumed to be one of plane strain; that is ε_z is assumed to be zero for the entire specimen.

(c) The adhesive is assumed to be an elastic layer in which the thickness variation of stresses is neglected. In formulating the adhesive a slight improvement is made over the conventional uncoupled tension-shear spring model by taking into account the effect of the average in-plane strain ε_x.

Partial reasons for adopting the particular analytical model for the adhesive joint are as follows:

(1) Generally, in adhesively bonded structures, the thickness of the adhesive is very small compared to the thicknesses of the adherends which, in turn, are small compared to the in-plane dimensions of the joint. The "plate" theory is known to deal quite satisfactorily with structures having such geometries.

(2) The plane problem can be solved in closed form (Ref. IV-1).

(3) The technique can be extended to treat adhesively bonded joints with complicated geometries and to take into consideration such effects as viscoelastic behavior of the adhesive (Ref. IV-2).

(4) Even though the model is not suitable for the calculation of a "stress intensity factor", it is suitable for the calculation of the "strain-energy-release rate".

(5) For one specimen geometry tested the tensile and shear stresses in the adhesive obtained from the plate model appear to be in good agreement with those given by the finite element method (Ref. IV-1).

APPROACH

The two adherends are assumed to be "plates" under in-plane deformations and bending. The equalibrium equations for the lap and the strap adherend may be expressed as follows:

$$\frac{dN_{1x}}{dx} = \tau, \quad \frac{dQ_{1x}}{dx} = \sigma \quad \frac{dM_{1x}}{dx} = Q_{1x} - \frac{h_1 + h_o}{2}\tau \tag{IV-1}$$

$$\frac{dN_{2x}}{dx} = -\tau, \quad \frac{dQ_{2x}}{dx} = -\sigma, \quad \frac{dM_{2x}}{dx} = Q_{2x} - \frac{h_2 + h_o}{2}\tau, \tag{IV-2}$$

where for $i = 1$ and $i = 2$ N_{ix}, Q_{ix}, M_{ix}, are the stress and moment resultants in the lap and strap adherends, respectively, and τ and σ are the shear and the normal stress in the adhesive. The stress and moment resultants are related to the x, y-components of the displacements u_i, v_i and to the rotations β_{ix}, $(i = 1,2)$ by

$$\frac{du_i}{dx} = C_i N_{ix}, \quad \frac{dv_i}{dx} + \beta_{ix} = \frac{Q_{ix}}{B_i}, \quad \frac{d\beta_{ix}}{dx} = D_i M_{ix}, \quad (i=1,2) \tag{IV-3}$$

$$C_i = \frac{1-\nu_{ix}\nu_{iz}}{h_i E_{ix}}, \quad B_i = \frac{5}{6} h_i G_{ixy}, \quad D_i = \frac{12(1-\nu_{ix}\nu_{iz})}{h_i^3 E_{ix}} \tag{IV-4}$$

Assuming that y-dependence of the strains ε_x, ε_y, and γ_{xy} in the adhesive is negligible, from kinematical considerations it may be shown that

$$\varepsilon_y = \frac{v_1 - v_2}{h_o}, \gamma_{xy} = (u_1 - \frac{1}{2} h_1 \beta_{1x} - u_2 - \frac{1}{2} h_2 \beta_{2x}) / h_o,$$

$$\varepsilon_x = (\frac{du_1}{dx} - \frac{h_1}{2} \frac{d\beta_{1x}}{dx} + \frac{du_2}{dx} + \frac{h_2}{2} \frac{d\beta_{2x}}{dx})/2, \qquad \text{(IV-5)}$$

where h_o, h_1 and h_2 are the thicknesses of the adhesive, the lap adherend and the strap adherend, respectively. If E, and ν denote the elastic constants of the adhesive, its stress-strain relations may be expressed as

$$\varepsilon_y = \frac{1-\nu-2\nu^2}{E(1-\nu)} \sigma - \frac{\nu}{1-\nu} \varepsilon_x, \gamma_{xy} = \tau \frac{2(1+\nu)}{E} \qquad \text{(IV-6)}$$

By simple eliminations, Equations (IV-1)-(IV-6) may be reduced to a system of differential equations for the functions $\tau(x)$ and $\sigma(x)$ which can then be solved in closed form (see Ref. IV-1 for details).

Strain Energy Release Rate

In an elastic structure containing a flaw of "area" A, ignoring the dynamic effects, the energy balance Equation may be expressed as

$$G = \frac{d}{dA} (U-V) = \gamma_F$$

where U is the work done by the external forces, V is the stored elastic energy and γ_F is the fracture energy of the material. In Equation (IV-7) the left-hand side represents the externally added or internally released energy available for fracture, and γ_F is the measure of the fracture resistance of the material. If the bulk of the structure undergoes elastic

deformations, it is known that G is the same under "fixed grip" and "fixed load" conditions. Thus, G can be calculated similar to the crack closure energy by considering the advance of the debond front, and by assuming fixed grip conditions.

As the debond front advances by a length da, $dU = 0$ and dV (per unit crack front) may be calculated by relaxing the stress state in the adhesive for a volume $h_o\,(1.0)(da)$ and the surface tractions $\sigma(X)$ and $\tau(X)$ acting on the adherends along the debond area da to zero. The strain energy released by the adherends due to the relaxation of the tractions σ and τ may be expressed as

$$dV_1 = -\frac{1}{2}\,\sigma da\,(\delta_{t1} + \delta_{t2}) - \frac{1}{2}\,\tau da\,(\delta_{s1} + \delta_{s2}) \qquad \text{(IV-8)}$$

where δ_{ti} and δ_{si}, $(i=1,2)$ are the y and x-components of the displacements of the adherend surfaces at the debond region da due to the removal of the tractions σda and τda and the minus sign is due to the fact that during the release process, the directions of the forces and the displacements are opposite to each other.

The strain energy released from the relaxation to the adhesive may be obtained from

$$dV_2 = -\int_a^{a+da} dx \int_0^{h_o} dy \int_0^1 dz\, W \qquad \text{(IV-9)}$$

where W is the strain energy density in the adhesive. In the model used and for the plane strain problem under consideration, the adhesive stresses are assumed to be independent of y and z. Thus, Eq. (IV-9) can be expressed as

$$dV_2 = -Wh_o da = -\frac{1}{2}\,(\sigma_x \epsilon_x + \sigma_y \epsilon_y + \tau_{xy}\gamma_{xy})h_o da \qquad \text{(IV-10)}$$

where W is calculated at the debond front. For the problem under consideration we have (REF. IV-1):

$$dV_2 = -\frac{h_o}{2}\left[\frac{E\varepsilon_x^2(a)}{1-\nu^2} + \frac{\sigma^2(a)}{E}\frac{1-\nu-2\nu^2}{1-\nu} + \frac{\tau^2(a)\ 2(1-\nu)}{E}\right]da \qquad \text{(IV-11)}$$

where E, ν and G are the elastic constants of the adhesive and ε_x, σ, and τ are calculated at the debond front a.

We now observe that the plate theory would give the displacements in the adherends as follows:

$$\delta_{ti} \simeq \frac{oda}{E_i}\ ,\quad \delta_{si} \simeq \frac{\tau da\ (1-\nu_i)}{E_i}\ (i=1,2) \qquad \text{(IV-12)}$$

From Eqs. (IV-8) and (IV-12) it then follows that as da→o the strain-energy-release rate dV_1/da contributed by the adherends would approach zero. Since $dV = dV_1 + dV_2$ and dA = da (per unit debond front), from Eqs. (IV-7) and (IV-11) we obtain

$$G = \frac{d}{da}(U-V) = \frac{h_o}{2}\left[\frac{E\varepsilon_x^2(a)}{1-\nu^2} + \frac{1-\nu-2\nu^2}{1-\nu}\frac{\sigma^2(a)}{E} + \frac{\tau^2(a)\ 2(1-\nu)}{E}\right] \qquad \text{(IV-13)}$$

The strain-energy-release rate G calculated from Eq. (IV-13) would be equivalent to the conventional $G_I + G_{II}$. It should be noted that if at the debond front the adhesive is in compression (which generally is the case if the bending stiffness of the lap adherend is greater than that of the strap adherend and if there is no transverse constraint in the strap adherend), then Eq. (IV-13) should be modified as follows:

$$G = G_{II} = \frac{h_o}{2}\left[\frac{E\varepsilon_x^2(a)}{1-\nu} + \frac{\tau^2(a)2(1+\nu)}{E}\right], \quad (\sigma(a) < 0) \qquad \text{(IV-14)}$$

In this case the problem is equivalent to $K_I = 0$ in a crack under mixed mode conditions, and the effect of possible crack surface friction is ignored.

RESULTS

As pointed out in the previous section, the plate model used in this study can give only the total strain-energy-release rate G rather than G_I and G_{II} separately. Furthermore, since plane strain conditions are assumed to prevail in z-direction, in the present solution $G_{III} = 0$. For the transversely constrained loading condition and dimensions shown in Figs. IV-1 and IV-2 the results for the complete range of the debond length are given in Table IV-1 (see also Table IV-2). Here the adherends are assumed to be aluminum ($E = 72.450$ MPa, $\nu = 0.33$) and the elastic constants of the adhesive are $E = 1932$ MPa, $\nu = -.40$. To indicate the overall trend, the results are also shown in Fig. IV-3.

From the expression for the strain-energy-release rate given by Eq. (IV-13) and from the calculated results, it was observed that the contribution of the first term (involving ε_x) to G is approximately two orders of magnitude smaller than that of the remaining terms. Thus, if the effect of ε_x is neglected, the second and third terms in Eq. (IV-13) may be interpreted as G_I and G_{II}, respectively. Partial results giving the individual contributions of the terms involving σ, τ, and ε_x in Eq. (IV-13) are given in Table IV-2 and are labeled as G_I, G_{II}, and G_ε, respectively. Note that G is the sum of these three terms.

Fig. IV-1 also shows the strain-energy-release rate for the cracked lap-shear specimen without the transverse end constraint. In this problem the transverse shear force Q at the end is zero and the specimen is free to

"bend". Consequently, the normal stress in the adhesive is zero for the specimen with equal thickness adherends and compressive for the specimen with unequal thickness adherends. Thus, for these two specimens G is calculated from Eq. (IV-14). A peculiar result observed in these calculations was that in varying the debond length a from zero to 229 mm, G turned out to be constant, namely

$$G = 45\ J/m^2 \text{ for CLS.A}(h_1 = h_2),$$

$$G = 74\ J/m^2 \text{ for CLS.B } (h_1 = 2h_2)$$

In the plate model adopted in this study, it is assumed that in the "debonded" part of the joint the adhesive layer is completely unloaded. Therefore, in this model, the results are not sensitive to the location of the "crack" in the adhesive and the calculated "crack opening displacement" does not have the conventional meaning.

REFERENCES

[IV-1] Delale, F. and Erdogen, F.: "Stresses in Adhesively Bonded Joints: A Closed-Form Solution", J. Composite Materials, Vol. 15, pp. 249-271, 1981.

[IV-2] Delale, F. and Erdogen, F.: "Viscoelastic Analysis of Adhesively Bonded Joints", J. Appl. Mech., Vol. 48, Trans. ASME, pp. 331-338, 1981.

TABLE IV-1

Calculated Strain Energy Release Rates
With Debond in Middle of Adhesive

J/m^2

Debond Length in. / mm.	0.1 / 2.54	0.25 / 6.35	1.0 / 25.40	4.0 / 101.60
CLSA				
G_I	39	43	62	51
G_{II}	145	151	180	163
G_ε	0.3	0.3	0.4	0.4
G_T	184	195	243	214
CLSB				
G_I	102	110	126	19
G_{II}	284	294	311	175
G_ε	0.6	0.6	0.6	0.3
G_T	387	404	437	194

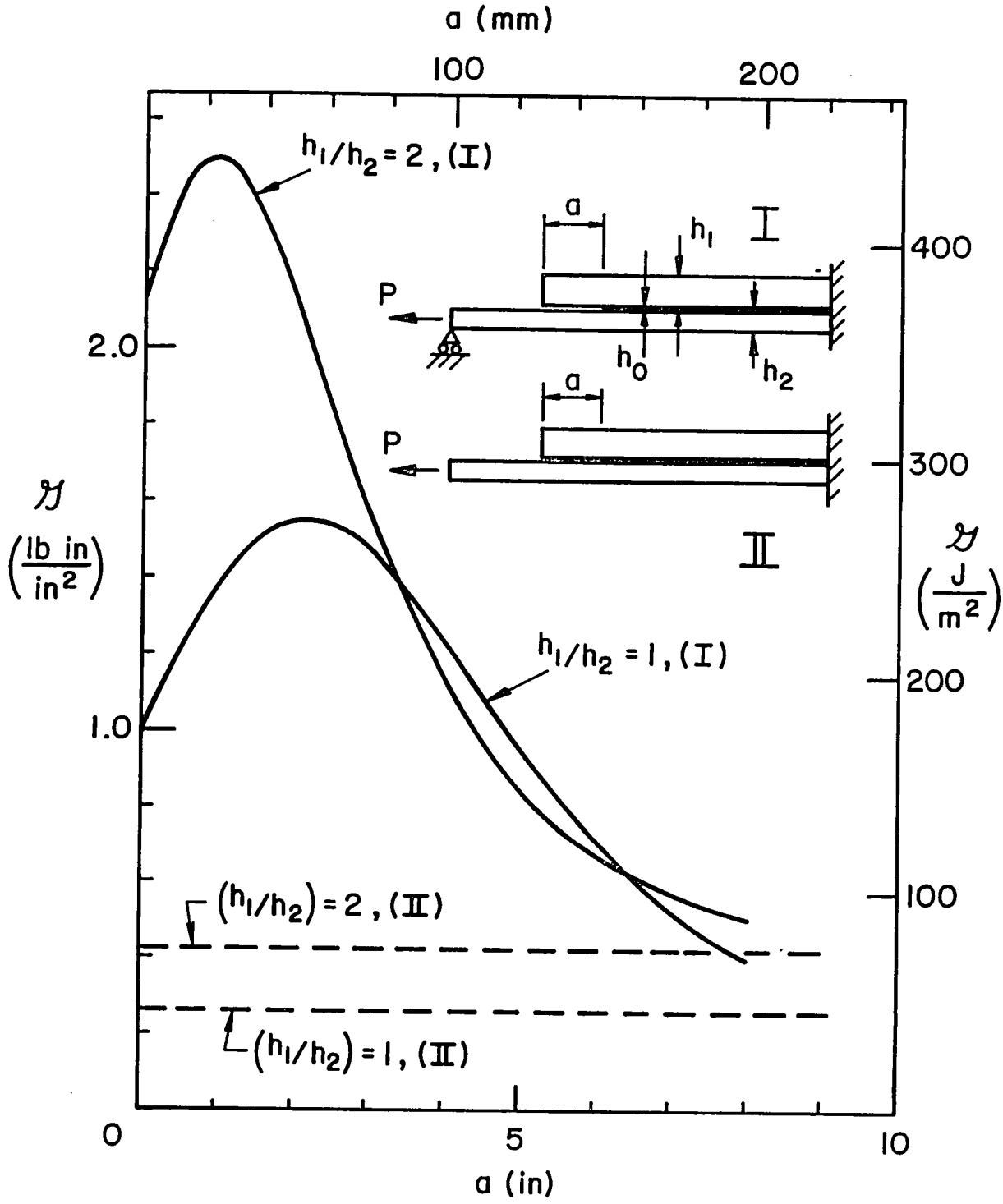

Figure IV-1. Strain energy release rate vs. debond length, a, in a constrained (insert figure I) and unconstrained (insert figure II) cracked lap shear specimen.

APPENDIX V

R. A. Everett, Jr.* and J. D. Whitcomb
NASA Langley Research Center
Hampton, VA 23665

APPROACH

To analyze the cracked-lap-shear (CLS) bonded joint configurations specified in this round robin, a two-dimensional finite element program called GAMNAS (Geometric and Material Nonlinear Analysis of Structures) was used. This program was developed at NASA Langley to support fracture mechanics studies of debonding and delamination and is documented in Refs. V-1 and V-2. This study used a nonlinear geometric analysis assuming plane strain conditions. To calculate strain-energy-release rates, GAMNAS uses a crack closure technique like that reported in Ref. V-3. This is done by using the forces transmitted through the node at the crack tip and the relative displacements of the two nodes on the crack boundary closest to the crack tip to calculate the energy required to close the crack.

No special crack tip elements are used in GAMNAS. For this analysis a 4-node isoparametric quadrilateral element was used. This finite element program has options for full and selective reduced integration. In this analysis selective reduced integration was used to improve the element's performance in modeling bending type deformations.

The mesh for the CLSB specimen with a 101.6 mm debond is shown in Fig. V-1. All the analyzed configurations were modeled similarly. All models had about 1000 elements with the thickest adherend having 9 elements through-the thickness and the thinnest having 7. The adhesive had 4 elements through-the thickness. At the debond tip the elements had an aspect ratio of one with

---

* U.S. Army Aerostructures Directorate

the length of the element being 0.032 mm. The debond was modeled as a perfectly smooth crack between the second and third elements in the adhesive layer (in the middle of the adhesive).

RESULTS

The strain-energy-release rates calculated in this analysis are presented in Table V-1. Both linear and nonlinear results are given for mode I, mode II, and the total strain-energy-release rates at the four debond lengths analysed.

The most significanct observation from the results in Table V-1 is that the G_T calculated from the nonlinear geometric analysis is almost constant with debond length, whereas, the linear results show G_T to vary with debond length with a maximum value at one inch. The ratio of G_I/G_{II} behaves in a similar manner. In general, for both configurations the nonlinear value of G is less than the linear value. The results also show that the CLSB configuration with the thicker lap adherend gives a higher value of G_T.

REFERENCES

[V-1] Whitcomb, J. D. and Dattaguru, B., "User's Manual for GAMNAS (Geometric and Material Nonlinear Analysis of Structures", NASA TM 85734, Jan. 1984.

[V-2] Dattaguru, B., Everett, R. A., Whitcomb, J. D., and Johnson, W. S.: "Geometrically Nonlinear Analysis of Adhesively Bonded Joints", Journal of Engineering Materials and Technology, Vol. 106, Jan. 1984, pp. 59-65.

[V-3] Rybicki, E. F. and Kanninen, " A Finite Element Calculation of Stress Intensity Factors by a Modified Crack Closure Integral", Engineering Fracture Mechanics, Vol. 9, pp. 931-938, 1977.

TABLE V-1

Calculated Strain-Energy-Release Rate With Debond In Center Of Adhesive, J/m^2. Both Geometic Linear And Nonlinear Results Are Presented.

Debond length in. / mm.	0.10 / 2.54		0.25 / 6.35		1.0 / 25.4		4.0 / 101.6	
	linear	nonlin.	linear	nonlin.	linear	nonlin.	linear	nonlin.
CLSA								
G_I	37	39	44	39	60	39	47	40
G_{II}	145	147	149	149	180	151	163	152
G_T	182	186	193	187	240	189	212	193
CLSB								
G_I	100	51	110	51	123	53	19	46
G_{II}	284	221	291	222	312	226	175	217
G_T	383	271	401	273	434	279	194	263

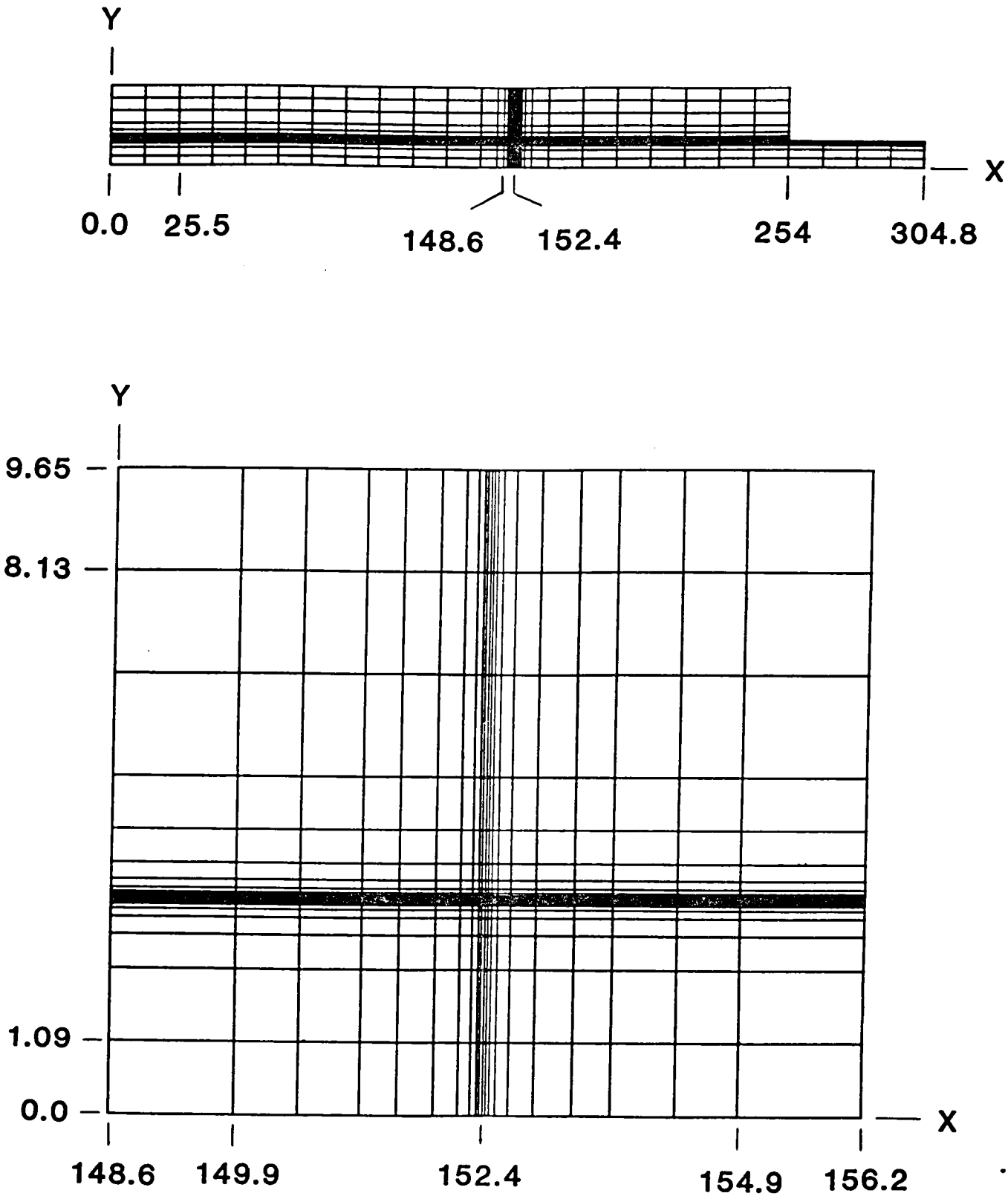

Figure V-1. Finite element mesh for 101.6 mm debond in the unsymmetric adherends specimen configuration.

APPENDIX VI

William L. Hufferd
United Technologies
Chemical Systems Division
San Jose, California

APPROACH

Linear elastic analyses of the two cracked lap shear geometries were conducted using two different finite element codes: TEXGAP (Ref. VI-1) and VISTA (Ref. VI-2). Geometrically nonlinear analyses were conducted for one cracked lap shear geometry using VISTA.

The version of TEXGAP used at CSD calculates stress intensity factors in one of three ways: (1) using a hybrid crack element, (2) using contour integration, and (3) using a singular crack element. The hybrid crack element was used in the current calculations. This element is based on a displacement formulation in which the displacements are interpolated over the boundary of the element and the stresses are interpolated over the interior of the element. Mode I and mode II stress intensity factors are calculated directly.

The hybrid element is an 11-node, square element with its local coordinate system located at the center of the element (i.e., the crack tip). The element may be used for plane stress or plane strain geometries or axisymmetric geometries at large radius. It has been reformulated for incompressible or nearly incompressible materials, and it includes thermal loadings, but excludes body forces. The crack surfaces within the element are assumed traction free.

The hybrid crack element used 15 interpolating, quadratic displacement functions for boundary displacements which insure interelement compatability with adjacent quadratic elements, and 19 different interpolating stress functions for the interior of the element which identically satisfy both

compatability and equilibrium. Symmetric and antisymmetric stress distributions are included as well as mode I and mode II stresses. The stress fields model the square-root singularity and also incorporate eigenvalues greater than one. The angular dependence of the stress distribution is also appropriately modeled.

VISTA is a finite element code for the solution of two dimensional (axisymmetric or generalized plane strain) quasistatic viscoelastic stress analysis problems with small strains and small or large displacements. The singular element used for fracture mechanics analysis with VISTA is based on the interpolating shape functions given by Stern (Ref. VI-3). It is a six-node subparametric triangle. The corner nodes are used for geometry interpolation and the midside and corner nodes are used for displacement interpolation. Thus, it is a straight sided element. The order of the singularity (one-half for linear elastic, isotropic materials) is input by the user. The displacements are quadratic along the side of the element opposite the singular point, thus conforming with the quadratic isoparametric elements in VISTA.

The implementation of the element in VISTA uses the standard element stiffness and load vector routines. Thus, the constitutive properties are handled by the same routines as regular elements so that any material can be used in the singular elements. The numerical integrations in the singular element use a specially derived quadrature rule.

The code outputs the coefficients of the displacement field; i.e.,

$$U'_x = \rho^{\lambda} f_u(\theta)$$

$$U'_y = \rho^{\lambda} f_v(\theta)$$

where λ is the order of the (user specified) singularity and ρ and θ are polar triangular coordinate. For the mixed mode problem in an isotropic linearly elastic solid with $\lambda = 1/2$, the plane strain near field displacements are given by:

$$U'_x = \frac{K_I}{G}\sqrt{\frac{\rho}{2\pi}} \cos\frac{\theta}{2}\left[1 - 2\nu + \sin^2\frac{\theta}{2}\right]$$

$$+ \frac{K_{II}}{G}\sqrt{\frac{\rho}{2\pi}} \sin\frac{\theta}{2}\left[2 - 2\nu + \cos^2\frac{\theta}{2}\right]$$

$$U'_y = \frac{K_I}{G}\sqrt{\frac{\rho}{2\pi}} \cos\frac{\theta}{2}\left[2 - 2\nu + \sin^2\frac{\theta}{2}\right]$$

$$+ \frac{K_{II}}{G}\sqrt{\frac{\rho}{2\pi}} \cos\frac{\theta}{2}\left[-1 + 2\nu + \sin^2\frac{\theta}{2}\right]$$

where G is the shear modulus and ν is Poisson's ratio for the material. Selecting the crack faces at $\theta = \pm\pi$ for evaluating K_I and K_{II} leads to the simple expressions:

$$K_I = \frac{E}{4(1-\nu^2)}\sqrt{2\pi}\, f_v(\theta)$$

$$K_{II} = \frac{E}{4(1-\nu^2)}\sqrt{2\pi}\, f_u(\theta)$$

These latter expressions were used to calculate stress intensity factors from VISTA output for $f_u(\theta)$ and $f_v(\theta)$, from which mode I and mode II strain-energy-release rates, G_I and G_{II}, respectively were calculated using:

$$G_I = \frac{(1 - \nu^2)\, K_I^2}{E}$$

$$G_{II} = \frac{(1 - \nu^2)\, K_{II}^2}{E}$$

DESCRIPTION OF ANALYSIS CONDUCTED

A typical deformed finite element model is shown in Fig. VI-1 for the CLS-B geometry with a 25.40 mm cohesive crack through the midplane of the adhesive layer. The model contains 397 elements. Four elements were used through the 5-mil thickness of the adhesive layer. The mesh in the neighborhood of the crack tip is shown in Fig. VI-2. The crack-tip region itself was modeled with eight singular triangular elements. The singular elements were overlaid with the hybrid crack element as shown in Fig. VI-3 for the TEXGAP analyses. All other finite element models for analyses of both crack lap shear geometries: CLS-A(3.18 mm thick lap and strap) and CLS-B (6.35 mm thick lap and 3.18 mm thick strap) were similar, except that the 4 × 4 fine mesh was moved with the crack tip for other crack lengths.

Linear elastic analyses were conducted for both CLS geometries for 2.54, 6.35, 25.4 and 101. 6 mm cohesive cracks in the adhesive. A geometrically nonlinear analysis was conducted for a 25.4 mm crack in the 6.35 mm lap and 3.18 mm strap CLS geometry (CLS-B). All analyses assumed plane strain conditions.

DISCUSSION OF RESULTS

One linear elastic analysis was conducted using VISTA to provide a baseline for comparison with TEXGAP analysis results. The two codes gave virtually identical stresses and displacements and the stress intensity factors calculated from the coefficients of the displacements from VISTA were within 2 percent of those obtained from the hybrid crack element used with the TEXGAP analyses.

Table VI-1 summarizes the calculated strain-energy-release rates. A slight maximum is observed at a crack length of about 25.4 mm. The thicker lap of CLS-B results in higher mode I and mode II values than is observed for the equal thickness adherends.

A geometrically nonlinear elastic analysis was conducted using VISTA in which the total load was applied in two load steps. Convergence for the first load step took six iterations, while that for the second took four iterations. A major effect of the nonlinear analysis was to "smooth" the distortion of the singular crack-tip elements on the free surface of the crack face. As a result, K_I dropped approximately 50 percent from the VISTA linear analysis while K_{II} changed only about 20 percent.

As a final remark, the absolute values of the stress intensities computed from the nonlinear analysis should be carefully interpreted. These calculations were made assuming that the order of the crack-tip singularity was one-half, the same as for a linear elastic analysis; and the calculations were made using the same displacement equations as used in a linear elastic analysis. The validity of these assumptions for this nonlinear problem is not known. In general, in this situation, more reliable results would be obtained from a patch-independent integral calculation, such as a J-integral, which has demonstrated validity for nonlinear elasticity problems.

REFERENCES

[VI-1] Becker, E. B. and Dunham, R. S., "Three Dimensional Finite Element Computer Program Development," AFRPL-TR-78-86, February 1979.

[VI-2] Becker, E. B., Chambers, R. S., Collins, L. R., Knauss, W. G., Liechti, K. M., and Romanko, J., "Viscoelastic Stress Analysis Including Moisture Diffusion for Adhesively Bonded Joints," AFWAL-TR-84-4057, Air Force Wright Aeronautics Laboratory, Dayton, OH, 1984.

[VI-3] Stern, M., "Families of Consistent Conforming Elements with Singular Derivative Fields," International Journal of Numerical Methods in Engineering, Vol. 14, 1979.

TABLE VI-1

Results With Debond In Middle Of Adhesive Using TEXGAP
(Geometric Linear)

J/m^2

Debond Length, in. / mm.	0.10 / 2.54	0.25 / 6.35	1.0 / 25.40		4.0 / 101.60
CLSA					
G_I	35	37	60		42
G_{II}	142	149	172		156
G_T	177	186	232		198
CLSB					
G_I	88	114	116	47*	12
G_{II}	282	298	310	207*	168
G_T	370	412	426	254*	180

*Calculated using VISTA (Geometic Nonlinear) at a=25.40 mm.

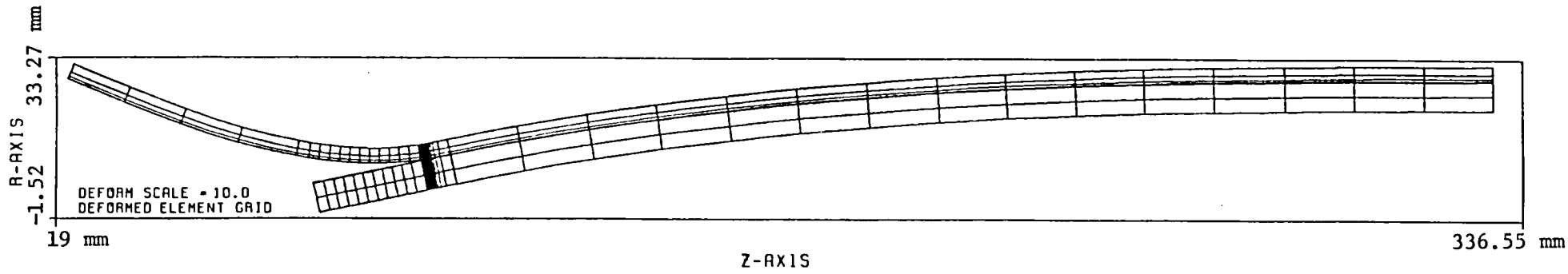

Figure VI-1. Deformed Finite Element Model of CLS-B (6.35 mm Lap and 3.18 mm Strap) Geometry with 25.4 mm Cohesive Crack in Adhesive Layer (Deformed Scale = 10)

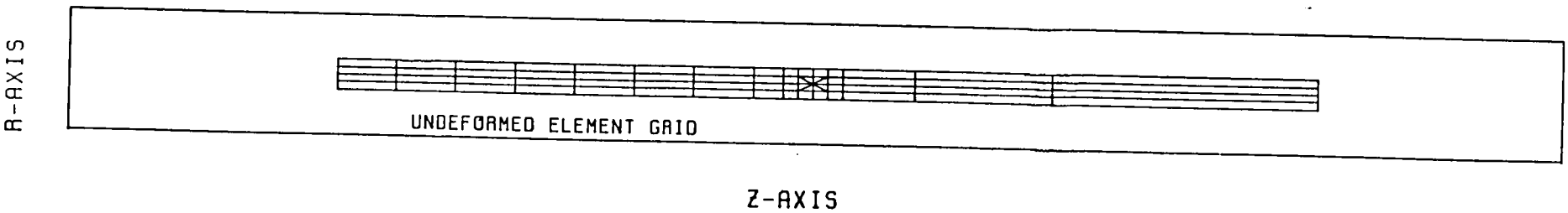

Figure VI-2. Crack-Tip Finite Element Model

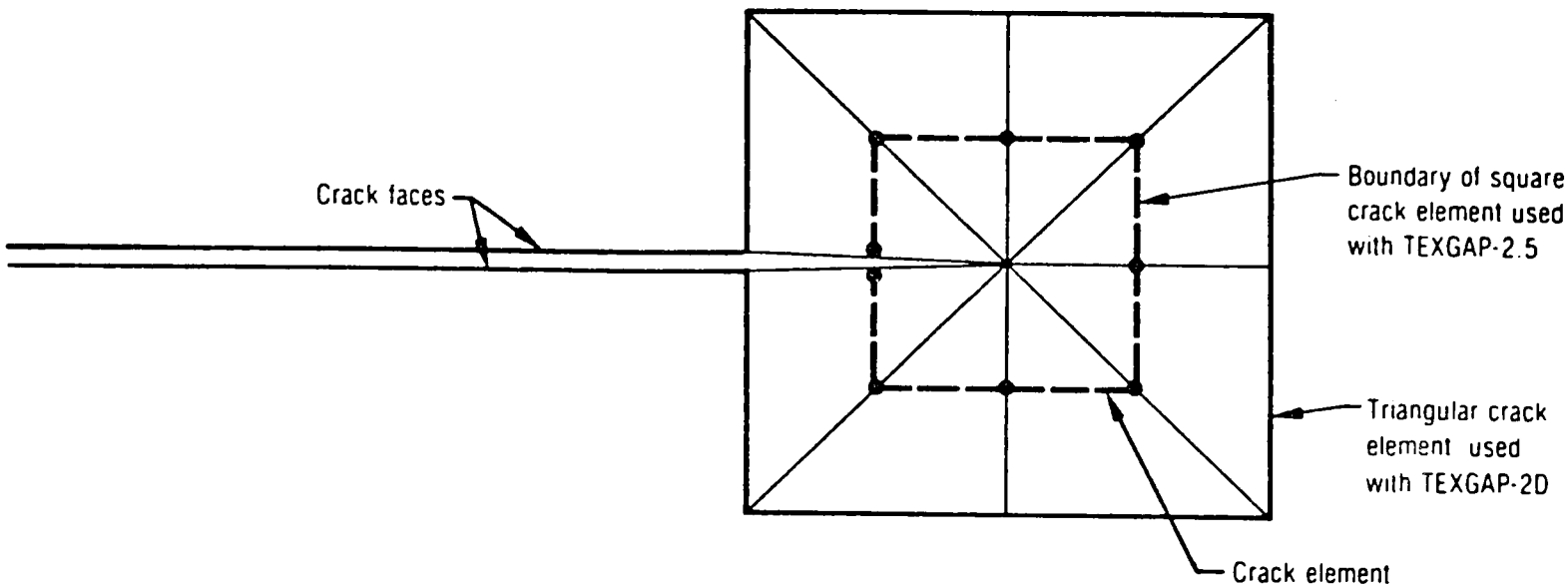

Figure VI-3. Details of the hybrid crack element overlaid singular triangular elements.

APPENDIX VII

George E. Law
General Dynamics
Fort Worth Division
Fort Worth, Texas

APPROACH

Non-linear geometric finite element analysis was performed with MSC/NASTRAN using "Solution 64". This is a non-linear geometry solution sequence for large displacement/small strain applications. The solution technique is based on the geometric stiffness approach. Details of this method are contained in Section 2.9 of the "MSC/NASTRAN Application Manual Volume 1", The MacNeal-Schwendler Corporation, Los Angeles, California, May 1983.

The two-dimensional finite-element model constructed for the analysis of the cracked lap shear specimen analysis is shown in Fig. VII-1. Isoparametric 3-node triangles and 4-node quadrilateral elements were employed in this model. The model was constructed using the load and out-of-plane directions to describe the 2D space. A state of plane stress was assumed. Fig. VII-1 shows the outline of the exterior surface of the model accentuating the crack line. A blow-up of the mesh at the crack tip area is also shown. Two models were made: one with a short, incomplete glue line and the second in which the complete glue line was modeled downstream from the crack tip. The elements in the crack-tip region were 0.0159 × 0.0159 mm.

The boundary conditions applied to the model were

$$u(0,y) = 0$$

$$v(0,0) = 0$$

$$v(L,0) = 0$$

The loading was applied as a tensile force of 2268 kg. (2500 lb.) at $x = L$; the force was uniformly distributed through the thickness of the model.

The modified crack closure technique (Ref. VII-1) was used to calculate the mode I and mode II components at the crack tip. Referring to Fig. VII-2, the nodal forces at "f" and the displacements at the first upstream nodes, "g" and "h", are combined to calculate the work to close the crack. The mode I and mode II components of the energy release rate are calculated as

$$G_I = F_y \, dv/2\Delta a$$

$$G_{II} = F_x \, du/2\Delta a$$

where

$$dv = v_g - v'_h$$

$$du = u_g - u'_h$$

F_x and F_y are the forces in the respective X and Y directions that resist the crack against opening, and Δa is the distance between node "f" and nodes "g" and "h" in the undeformed state.

In the case of the non-linear geometric analysis, the X- and Y- axes for the mode I and mode II components must be defined in the deformed state. Fig. VI-3 shows the relations required to determine a new X' -Y' coordinate system aligned with the crack. The results of the finite element analysis are transformed into the X' -Y' coordinate system through standard tensor transformations and the mode I and mode II components of the energy release rate are then calculated.

RESULTS

Two glue line models were used in this analysis. The short glue line model was found to produce erroneous results when compared with the full glue

line model. This short glue line model was exercised for all of the analysis cases of the round robin. Those results, although erroneous in magnitude, are presented in Table VII-1 to describe trends in the CLS analysis. The full glue line model was only exercised for two cases of the round robin. Since the results for that analysis agreed with results of other round-robin participants using nonlinear geometric analysis, it is inferred that all of the other cases would also agree.

Table I presents the energy release rates calculated for the equal thickness and unequal thickness adherend configurations. These values were calculated from the short glue line model and are only of value in that the trend of the analysis is represented. Two observations can be made from these results: the unequal thickness adherend shows greater mode II than the equal thickness adherend coupon, and the calculated energy release rates are essentially constant with crack length except for a slight perturbation in the short crack length range. The increase in the mode II component with increase in the thickness of the lap of the coupon is a direct result of increased stiffness (EA) of the lap. The increase in lap stiffness causes greater shear transfer across the bondline.

The relationship between energy release rate and crack length can be described based on concepts of self-similar crack propagation. For long crack lengths, the highly stressed zone-surrounding the crack tip does not interact with the end boundaries. Also, since the crack is parallel to the load direction, the net section is not reduced. Thus, it is inferred that the energy release rate should be independent of crack length. For the short crack lengths considered, the length of the crack is on the same magnitude as the thickness of the adherends. In this case, interactions between the stresses

around the crack tip and the boundary conditions, particularly the free boundary at the end of the lap, can be anticipated.

Table VII-2 gives the full glue line model results obtained for the constant thickness adherend case in the short (2.54 mm) and long (101.6 mm) crack length configurations. For the short and long crack length cases, Figs. VII-4 and VI-5 respectively show the relationship between the calculated energy release rates and the number of iterations in the nonlinear solution. Iteration number 1 represents the linear solution and numbers 2, 3, 4, and 5 represent each nonlinear iteration. These figures show that the solution for the energy release rate converges after two nonlinear iterations demonstrating that a linear solution is invalid.

Conclusions of this study are that the energy release rate is relatively constant with crack length in the cracked-lap-shear specimen. Also, the full glue line must be modeled in the adhesive CLS coupon to obtain proper internal shear transfer in the analysis.

REFERENCES

[VII-1] Rybicki, E. F.; and Kanninen, M. F.: "A Finite Element Calculation of Stress Intensity Factors by a Modified Crack Closure Integral", Engineering Fracture Mechanics, Vol. 9, 1977, pp. 931-938.

TABLE VII-1

Calculated Strain Energy Release Rates For Short Bondline*
With Debond In Middle Of Adhesive
(*Use for analysis trends only)

J/m^2

Debond Length				
in.	0.10	0.25	1.0	4.0
mm.	2.54	6.35	25.40	101.60
CLSA				
G_I	35	36	36	37
G_{II}	83	84	85	6
G_T	118	120	121	123
CLSB				
G_I	36	38	37	33
G_{II}	124	128	127	124
G_T	160	166	164	157

TABLE VII-2

Calculated Strain Energy Release Rates For Full Glue Line
With Debond In Middle Of Adhesive

J/m^2

Debond Length				
in.	0.10	0.25	1.0	4.0
mm.	2.54	6.35	25.40	101.60
CLSA				
G_I	45	--	--	47
G_{II}	176	--	--	181
G_T	221	--	--	228

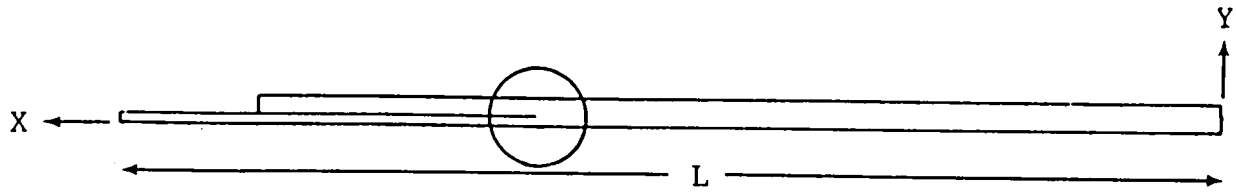

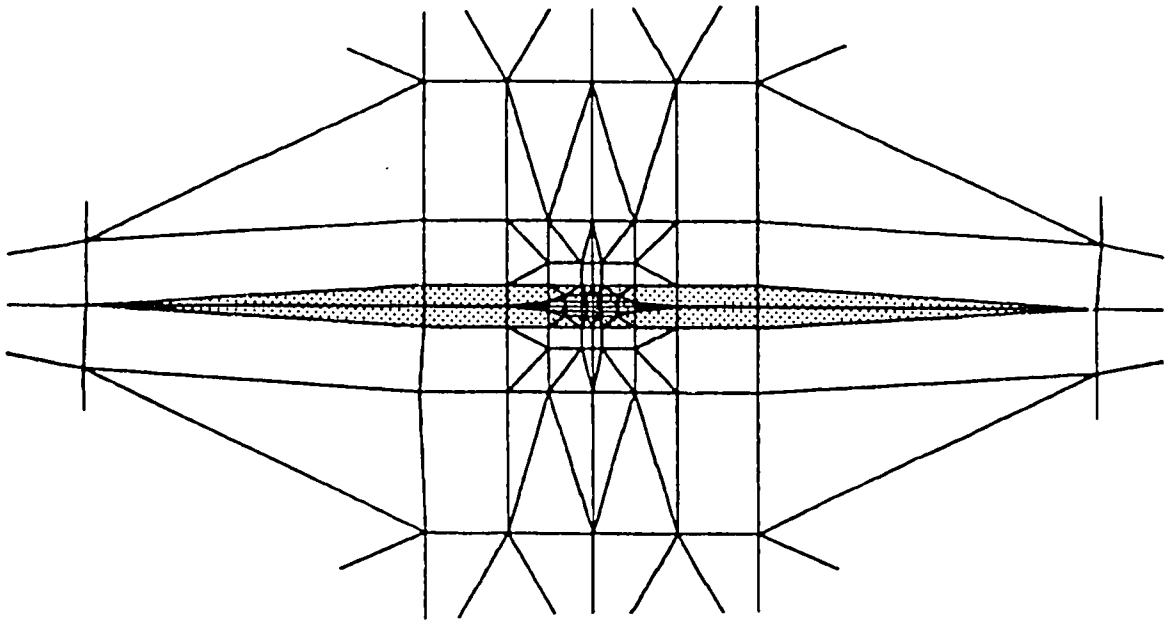

SHORT GLUE LINE

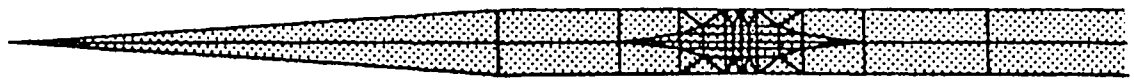

FULL GLUE LINE

Figure VII-1. Finite element models for the cracked lap shear specimen.

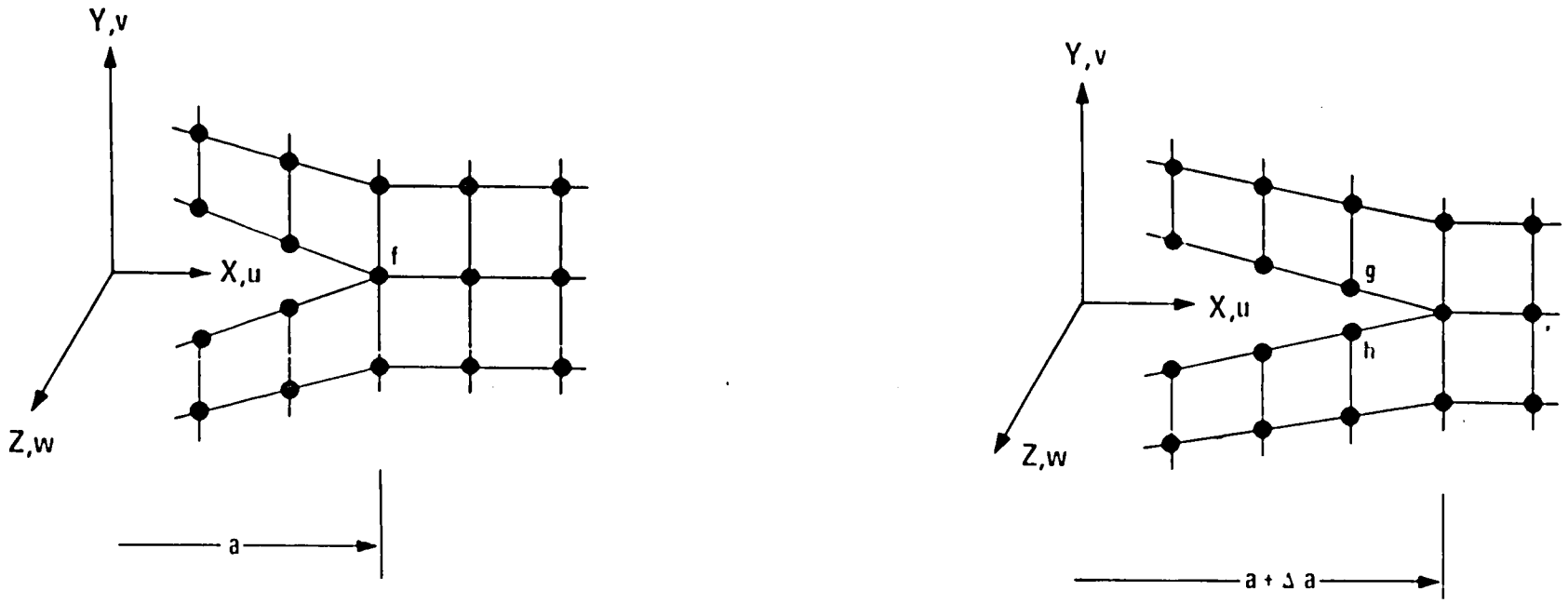

WORK TO CLOSE CRACK

$$W = 1/2\ \tilde{F} \cdot \tilde{d}$$

MODE I ENERGY RELEASE RATE

$$G_I = \frac{F_y \cdot dV}{2\Delta a}$$

B60575

Figure VII-2. Mesh at the crack tip.

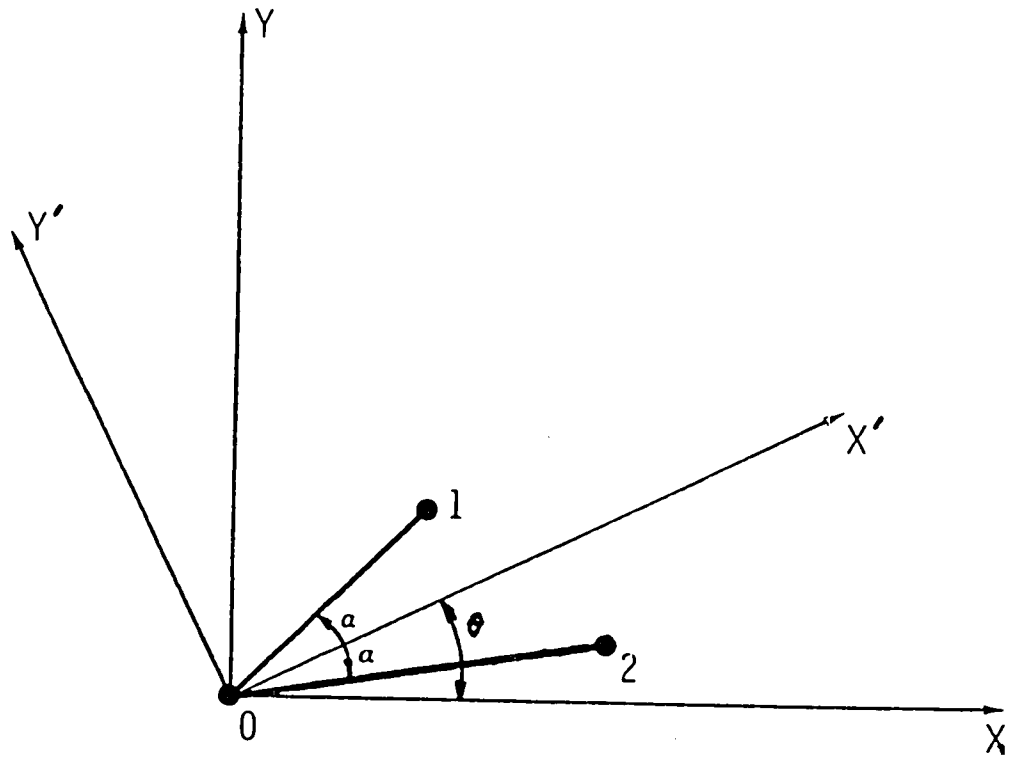

$$\theta = \tfrac{1}{2}\left[\text{TAN}^{-1}\left(\frac{V_2-V_0}{U_2-U_0+\Delta A}\right) + \text{TAN}^{-1}\left(\frac{V_1-V_0}{U_1-U_0+\Delta A}\right)\right]$$

Figure VII-3. Nonlinear analysis requires rotated crack tip geometry.

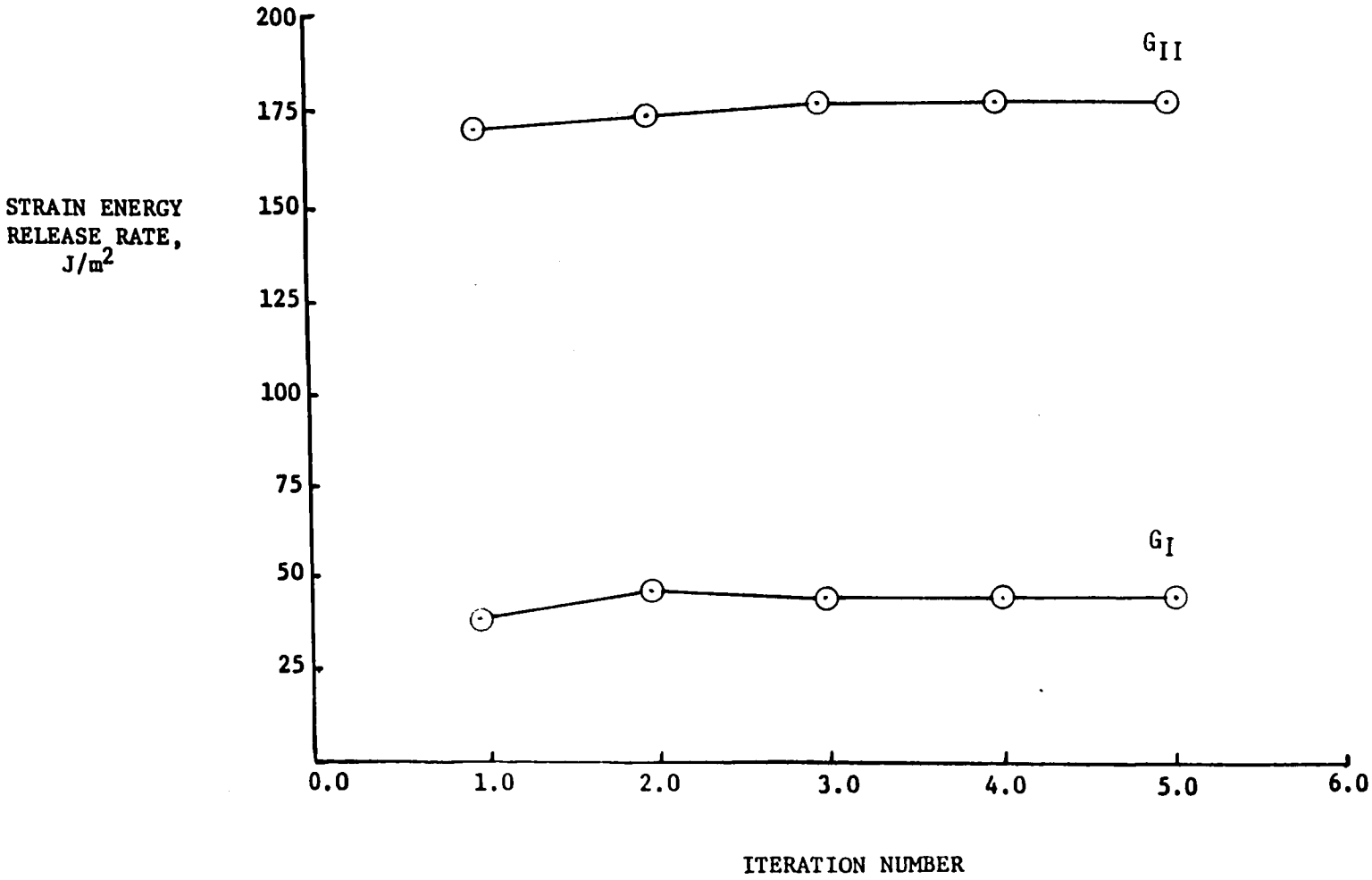

Figure VII-4. Convergence study for full glue line model-crack length a = 2.54 mm.

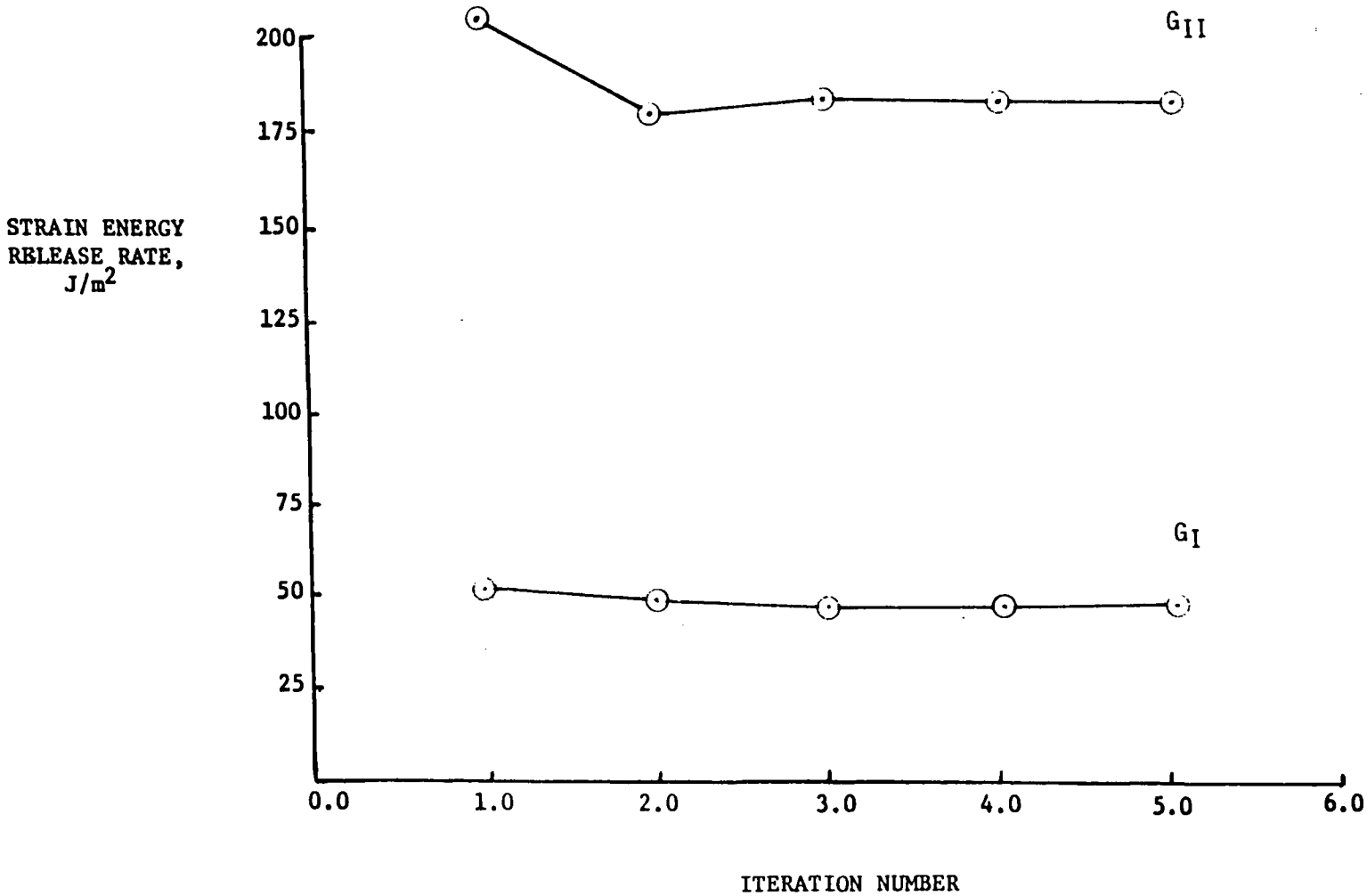

Figure VII-5. Convergence study for full glue line model-crack length a = 101.6 mm.

APPENDIX VIII

Charles J. Lof
National Aerospace Laboratory NLR
The Netherlands

APPROACH

A finite element program, ASKA (Ref. VIII-1) using three-dimensional strain elements (isoparametric) was used. K- and G- values are assumed to be related to displacements in the crack tip fields according to linear elastic fracture mechanics theory as described by Paris and Sih [VIII-2].

At the debond frontline, elements are applied with singular strain field at the tips (subnet 1). Other subnets (2 ... 5) consist of normal hexagonal 27-node elements. The debond size is varied by changing x-coordinates of the subnets in front of or behind the debond tip. The mesh is shown in Fig. VIII-1. G_I, G_{II}, and G_{III} are derived from K-values by Eq. (VIII-1) for mode I

$$G_I = K_1^2 \cdot \frac{1 - \nu^2}{E} \qquad \text{(VIII-1)}$$

K_1 is derived from displacements of nodes close to the debond tip, using Eq. (VIII-2).

$$K_I(r) = \frac{(u_1 - u_2)}{\sqrt{r}} \cdot \frac{E\sqrt{2\pi}}{8(1-\nu^2)} \qquad \text{(VIII-2)}$$

where u_1, u_2 are displacements at a distance r from the debond tip at the lap- or strap-side, respectively. The K_1-value at the tip is found by linear extrapolations of $K_1(r)$-values, especially from nodes of the crack tip elements. Similar formulas [VIII-1, VIII-2] are valid for mode II and mode III within the latter case: $(1+\nu)$ instead of $(1-\nu^2)$.

RESULTS

Table VIII-1: G-values are derived for 3 positions along the debond line across the specimens width, (z = 0 is the mid-plane of the bar). The G_{Total}-value, however, is derived using the virtual crack extension method [VIII-2] and the equation:

$$G = \frac{dU}{dA} \qquad \text{(VIII-3)}$$

where dU is the elastic energy variation by a very small local cracksize variation dA.

$$dU = \bar{u}\,[S - S^*]\underline{\bar{u}}$$

where $\bar{u}$ is the displacement vector and $[S - S^*]$ is the variation of the stiffness by virtual debond variation.

This total energy release value is expected to be considerably more accurate than the separate G_I, G_{II}, G_{III}-values obtained. However, the distribution over three modes can not be found in this way.

With respect to the total strain-energy-release rate results (Table VIII-1) we propose some adaption in order to properly compare these three-dimensional results with other two-dimensional data. Therefore, a "weighted average" of these results for discrete positions along the debond-zone frontline is proposed in the following form:

$$G_{tot(av)} = .4\ G_{tot(z=0)} + .5\ G_{tot(z=.4)} + .1\ G_{tot(z=.5)}$$

Different factors refer to different areas of virtual debond extensions (Fig VIII-2). The corrected results are given in Table VIII-2.

A remarkable effect found by the three-dimensional calculation is the "closure" of the debond-opening at the edges of the specimen, as seen by detail-observations of cross-sectional deformations of both adherends, in a plane very close behind the debond tip (Fig. VIII-3). Local G_I-values decrease rapidly from the mid-plane towards the side of the bar, whereas G_{III}-values increase.

Unfortunately, this phenonema was not studied in more detail, i.e. by using finer meshes, or non-linear calculation.

REFERENCES

[VIII-1] Lof, C. J., ASKA Part 1 - Crack Analysis User's Reference Manual. NLR TR 79041 U, May 1979.

[VIII-2] Paris, P. C. and Sih, C.: "Stress Analysis of Cracks". ASTM STP 381, June 1964.

TABLE VIII-1

Calculated Strain Energy Release Rates
With Debond In Middle Of Adhesive

J/m^2

Debond Length,												
in.	0.10			0.25			1.0			4.0		
mm.	2.54			6.35			25.40			101.60		
$Z/_{1.0 \text{ in.}}$	0 mid	.4	.5 side	0 mid	.4	.5 side	0 mid	.4	.5 side	0 mid	.4	.5 side
CLSA												
G_I	14	7	0	17	8	0	28	12	.05	23	10	0
G_{II}	119	105	122	135	113	136	154	131	155	141	115	136
G_{III}	0	3	33	0	13	38	0	16	47	0	16	43
G_T	205	187	194	224	208	217	281	255	255	247	222	222

TABLE VIII-2

Total Strain Energy Release Rate for CLSA

Debond length a, mm	G_{tot} (averaged) J/m^2
2.54	1.95
6.35	216
25.40	266
101.60	232

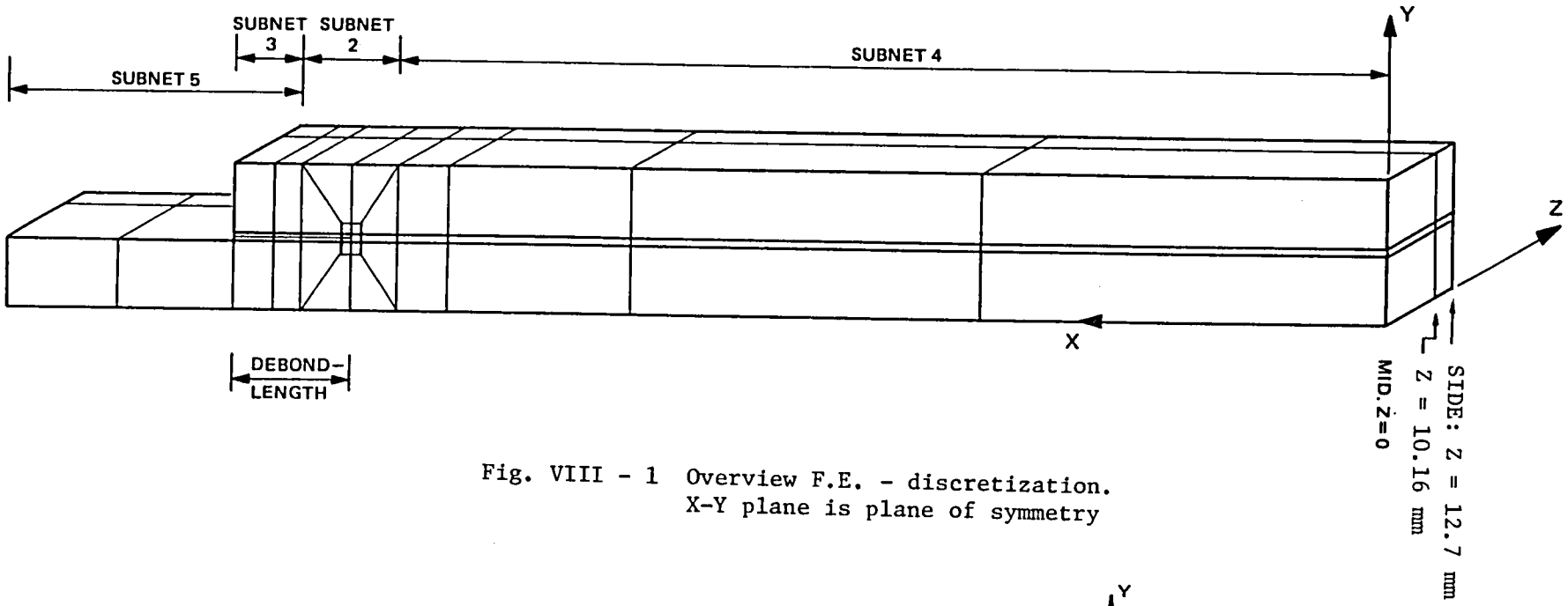

Fig. VIII - 1 Overview F.E. - discretization.
X-Y plane is plane of symmetry

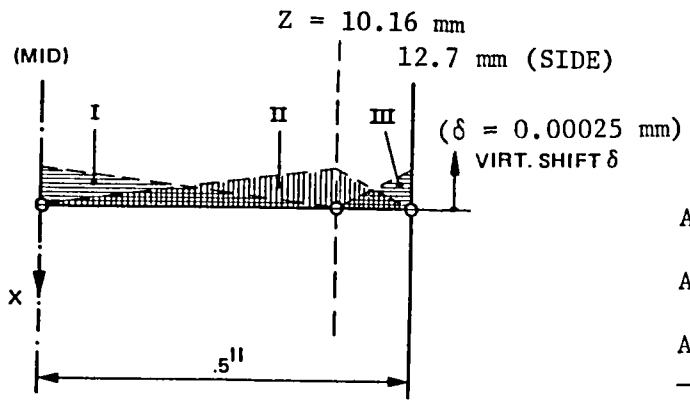

$$A_I = \delta * 5.00$$

$$A_{II} = \delta * 6.35$$

$$A_{III} = \delta * 1.27$$

$$A_{tot} = \delta * 12.7 \text{ mm}^2$$

Fig. VIII - 2 Debond frontline virtual shift area discretization

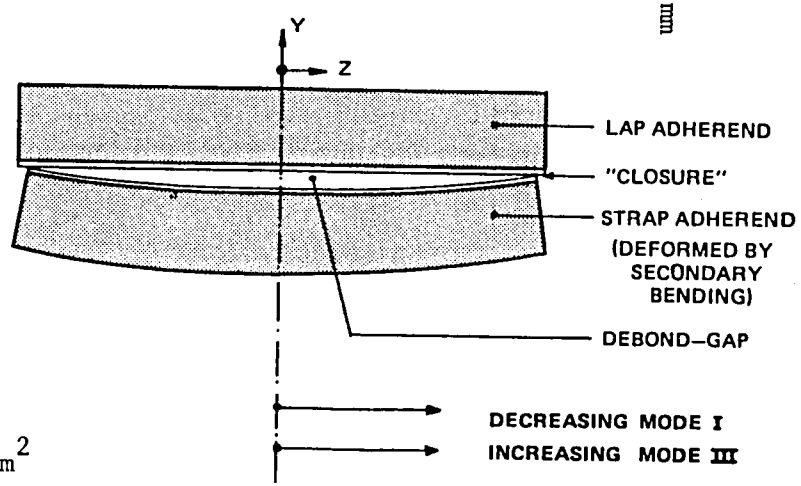

Fig. VIII - 3 Cross-sectional deformation

APPENDIX IX

S. Mall
Department of Engineering Mechanics
University of Missouri
Rolla, MO

APPROACH

The analysis of cracked-lap-shear specimens requires a geometric nonlinear method [IX-1, IX-2]. In the present approach, this nonlinear analysis was conducted by combining a simple nonlinear analysis (based on strength-of-materials theory) with a linear finite element analysis in the following manner [IX-3]. Figure IX-1(a) shows the cracked-lap-shear specimen which is to be analyzed with a geometric nonlinear method to account for the deformation which responds nonlinearly to the applied load geometry. Figure IX-1(b) shows a small region of this specimen near the debond front. This region near the debond front can be analyzed with a linear method provided moments, axial and shear loads acting on the boundary are obtained from a nonlinear analysis.

A nonlinear analysis based on a simple strength-of-materials theory was developed to compute moments, axial and shear loads acting on the boundary of the small region of the CLS specimen as shown in Fig. IX-1(b). This nonlinear analysis is the extension of a previous analysis [IX-4]. The previous analysis was for an infinitely long CLS specimen (i.e. independent of debond length), while the present one accounts for the finite length of the specimen and the debond. Fig. IX-2 shows the CLS specimen and the deformation of

its centroidal axis. From the simple beam theory, the following expressions for lateral deflection of centroidal axis were obtained.

$x > 0$

$$y(x) = \frac{(\bar{y}_2-\bar{y}_0)\lambda_0\coth(\lambda_0 \ell_0)}{\lambda_2\coth(\lambda_2\ell_2) + \lambda_0\coth(\lambda_0 \ell_0)} \cdot \frac{\sinh(\lambda_2 \ell_2-\lambda_2 x)}{\sinh(\lambda_2\ell_2)}$$

$x < 0$

$$y(x) = \frac{-(y_2-y_0)\lambda_2\coth(\lambda_2 \ell_2)}{\lambda_2\coth(\lambda_2\ell_2) + \lambda_0\coth(\lambda_0 \ell_0)} \cdot \frac{\sinh(\lambda_0 \ell_0-\lambda_0 x)}{\sinh(\lambda_0\ell_0)}$$

$$\lambda_2 = \sqrt{p/(EI)_2}$$

$$\lambda_0 = \sqrt{p/(EI)_0}$$

Using the above equations, the moments, axial and shear loads acting on the small region shown in Fig. IX-1(b) were computed. Thereafter, this region with computed boundary loads and moments was analyzed with a two-dimensional linear elastic finite element analysis.

The finite element mesh consisted of 510 four-node, isoparametric quadrilateral elements and had 1200 degrees for freedom. The length of region analyzed with FEM was 6.35 mm on each side of debond front (i.e. total length of 12.7 mm). The analysis was conducted under plane strain condition. The adhesive was modeled with four layers of elements. The smallest element size near the crack tip was 0.0318 × 0.0318 mm. The strain-energy-release rates G_T, G_I, and G_{II} in the FEM analysis were computed using a virtual crack closure technique (Ref. IV-5).

RESULTS

The computed strain-energy-release rates (G_T, G_I, and G_{II}) for both CLS A and CLS B specimens are presented in Table IX-1.

DISCUSSION

A simple approach for analysing the geometric nonlinear problem of the CLS specimen is suggested by combining a simple nonlinear analysis (based on the strength-of-materials theory) and linear finite element analysis.

REFERENCES

[IX-1] Dattaguru, B.; Everett, R. A., Jr.; Whitcomb, J. D.; Johnson, W. S.: "Geometrically Nonlinear Analysis of Adhesively Bonded Joints", Journal of Engineering Materials and Technology, Vol. 106, Jan. 1984, pp. 59-65.

[IX-2] Mall, S.; Johnson, W. S.; and Everett, R. A., Jr.: "Cyclic Debonding of Adhesively Bonded Composites", Adhesive Joints, K. L. Mittal, Ed; Plenum Press, New York, 1984, pp. 639-658.

[IX-3] Whitcomb, J. D., "Strain-Energy Release Rate Analysis of Cyclic Delamination Growth in Compressively Loaded Laminates," in Effects of Defects in Composite Materials, ASTM STP 836, American Society for Testing and Materials, Philadelphia, 1984, pp. 175-193.

[IX-4] Brussat, T. R.; Chiu, S. T.; and Mostovoy, S.: "Fracture Mechanics for Structural Adhesive Bonds", AFML-TR-77-163, Air Force Materials Laboratory Wright Patterson AFB, Ohio 1977.

[IX-5] Rybicki, E. F. and Kanninen, M. F.: "A Finite Element Calculation of Stress Intensity Factors by a Modified Crack Closure Integral" Engineering Fracture Mechanics, Vol. 9, No. 4, pp. 931-938, 1977.

TABLE IX-1

Calculated Strain Energy Release Rates With Debond In Middle Of Adhesive

(J/m^2)

Debond Length,					
in.	0.10	0.25	1.0	2.0	4.0
mm.	2.54	6.35	25.40	50.80	101.60
CLSA					
G_I	42	43	44	44	45
G_{II}	149	149	151	151	152
G_T	191	192	195	195	197
CLSB					
G_I	51	52	54	57	68
G_{II}	200	202	205	209	222
G_T	251	254	259	266	290

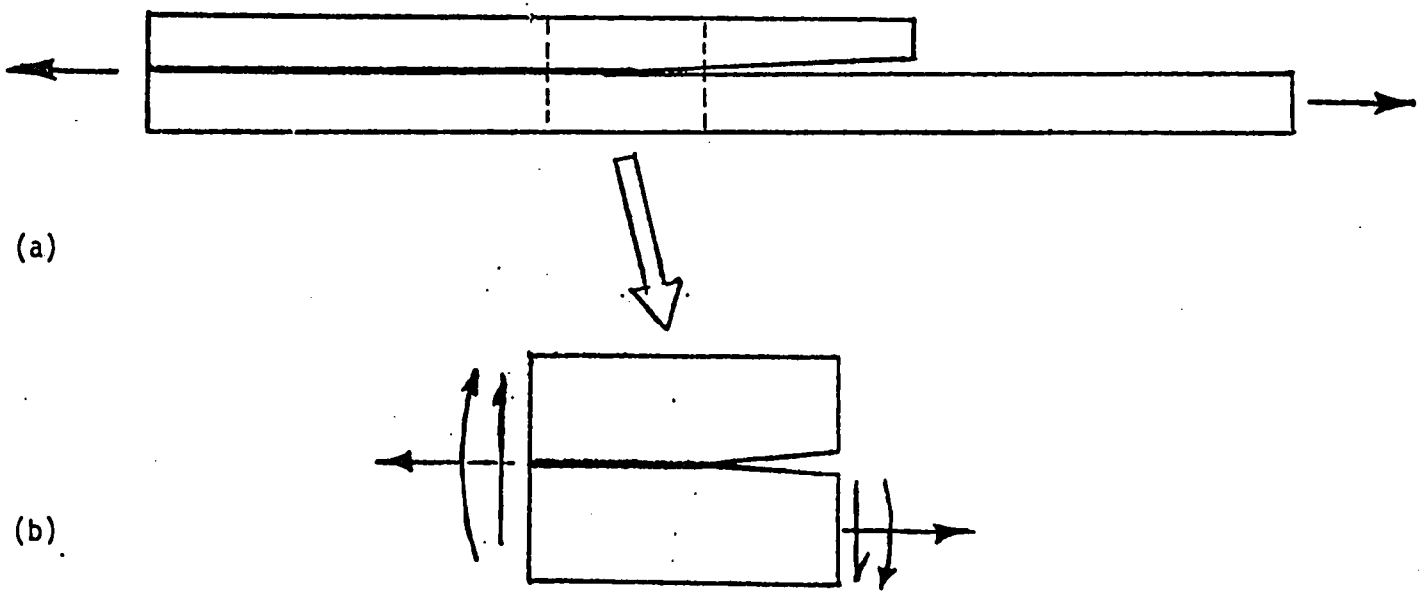

Figure IX-1. Simplified nonlinear analysis of cracked lap shear specimen.

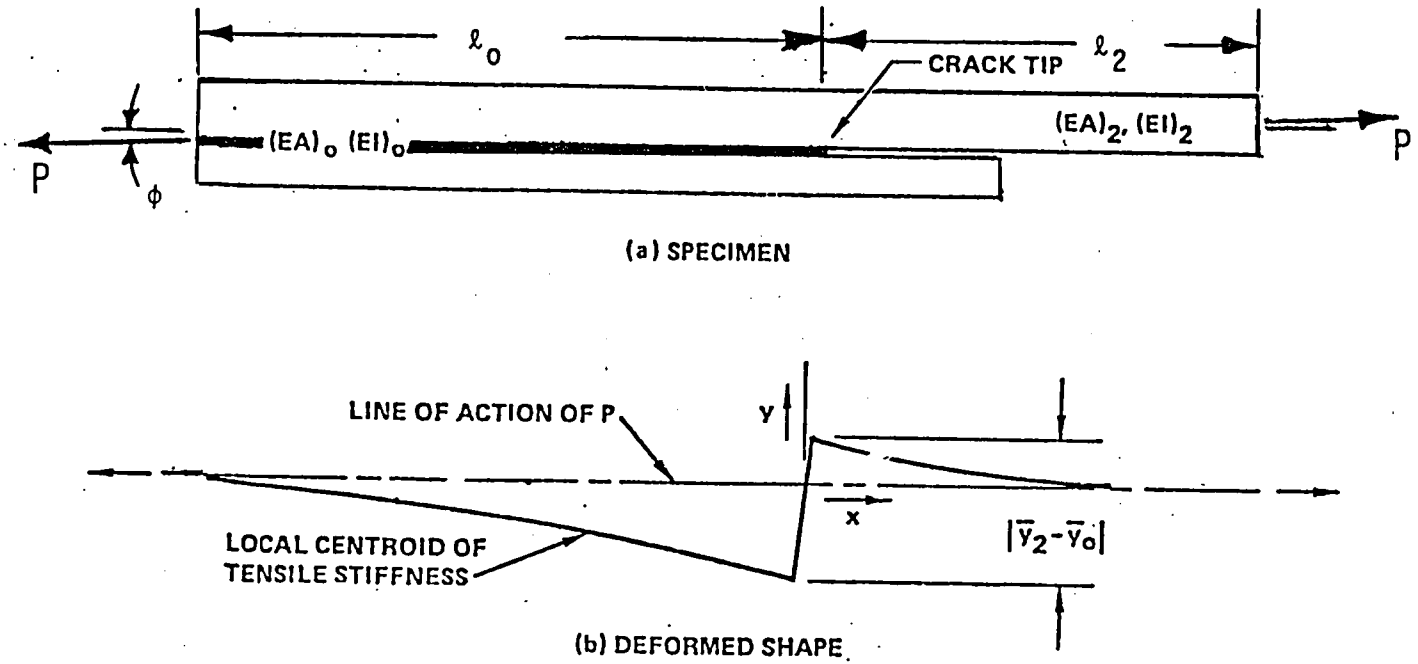

Figure IX-2. Cracked lap shear specimen and its deformed shape.

1. Report No.	2. Government Accession No.	3. Recipient's Catalog No.
NASA TM-89006		

4. Title and Subtitle	5. Report Date
Stress Analysis of the Cracked Lap Shear Specimens: An ASTM Round Robin	August 1986
	6. Performing Organization Code 506-43-11-04
7. Author(s)	8. Performing Organization Report No.
W. S. Johnson	
	10. Work Unit No.
9. Performing Organization Name and Address	
National Aeronautics and Space Administration Langley Research Center Hampton, VA 23665-5225	11. Contract or Grant No.
	13. Type of Report and Period Covered
12. Sponsoring Agency Name and Address	Technical Memorandum
National Aeronautics and Space Administration Washington, DC 20546	14. Army Project No.

15. Supplementary Notes Appendices by G. P. Anderson, L. P. Abrahamson, and K. L. DeVries; T. R. Brussat; B. Dattaguru and P. D. Mangalgiri; F. Erdogen and P. Joseph; R. A. Everett, Jr., and J. D. Whitcomb; W. L. Hufferd; G. E. Law; C. J. Lof; and S. Mall.

16. Abstract

This ASTM Round Robin was conducted to evaluate the state of the art in stress analysis of adhesively bonded joint specimens. Specifically, the participants were asked to calculate the strain-energy-release rate for two different geometry cracked lap shear (CLS) specimens at four different debond lengths. The various analytical techniques consisted of 2- and 3-dimensional finite element analysis, beam theory, plate theory, and a combination of beam theory and finite element analysis. The results were examined in terms of the total strain-energy-release rate and the mode I to mode II ratio as a function of debond length for each specimen geometry. These results basically clustered into two groups: geometric linear or geometric nonlinear analysis. The geometric nonlinear analysis is required to properly analyze the CLS specimens. The 3-D finite element analysis gave indications of edge closure plus some mode III loading. Each participant described their analytical technique and results. Nine laboratories participated.

17. Key Words (Suggested by Author(s))
Stress analysis
Cracked-lap-shear specimen
Mixed-mode
Strain-energy release rate
Bonded joints

18. Distribution Statement
Unclassified - Unlimited
Subject Category - 39

19. Security Classif. (of this report)	20. Security Classif. (of this page)	21. No. of Pages	22. Price*
Unclassified	Unclassified	86	A05

*For sale by the National Technical Information Service, Springfield, Virginia 22161